J. Fluid Mech. (2000), *vol.* 414, *pp.* 105–144. Printed in the United Kingdom

A general asymptotic theory of diffusion flames with application to cellular instability

By SALLY CHEATHAM† AND MOSHE MATALON

Engineering Sciences and Applied Mathematics, McCormick School of Engineering and Applied Science, Northwestern University, Evanston, IL 60208-3125, USA

(Received 14 June 1999 and in revised form 8 February 2000)

A general asymptotic formulation is presented for diffusion flames of large-activation-energy chemical reactions. In this limit chemical reaction is confined to a thin zone which, when viewed from the much larger diffusion scale, is a moving two-dimensional sheet. The formulation is not restricted to any particular configuration, and applies to conditions extending from complete combustion to extinction. The detailed structure of the reaction zone yields jump conditions that permit full determination of the combustion field on both sides of the reaction zone, as well as the instantaneous shape of the reaction sheet itself. The simplified system is subsequently used to study the intrinsic stability properties of diffusion flames and, in particular, the onset of cellular flames. We show that cellular diffusion flames form under near-extinction conditions when the reactant in the feed stream is the more completely consumed reactant, and the corresponding reactant Lewis number is below some critical value. Cell sizes at the onset of instability are on the order of the diffusion length. Predicted cell sizes and conditions for instability are therefore both comparable with experimental observations. Finally, we provide stability curves in the fuel and oxidant Lewis number parameter plane, showing where instability is expected for different values of both the initial mixture strength and the Damköhler number.

1. Introduction

The governing equations of chemically reacting flows consist of the fluid mechanics equations supplemented by equations expressing the mass balance of the various species involved in the chemical reaction (cf. Williams 1985). These equations are too difficult to solve either explicitly or by numerical and other approximate methods. In order to gain fundamental understanding of the complex nature of combustion problems, simplified theories are often suggested. These can be either obtained by physical reasoning, or derived in a more systematic way by means of asymptotic methods. There is a considerable advantage in deriving simplified theories: the formulation is self-consistent and identifies clearly the underlying assumptions involved which can be re-examined at a later stage.

For premixed systems several simplified theories have been derived and used in describing the propagation and dynamics of premixed flames and their stability. Examples which exploit the largeness of the activation energy parameter include the slowly-varying-flame (SVF) and the near-equidiffusional-flame (NEF) formulations (Buckmaster & Ludford 1982) which consider the Lewis number to be sufficiently

† Current address: Naval Research Laboratory, Washington, DC 20375, USA.

distinct from, or sufficiently close to 1, respectively. Another example is the thin-flame theory (Matalon & Matkowsky 1982, 1983) which is a NEF formulation that also takes advantage of the small diffusion-to-hydrodynamic length ratio. For non-premixed systems (diffusion flames) a general asymptotic formulation, applicable to an arbitrary three-dimensional flame, does not exist. The mixture fraction formulation (Peters 1983, 1986) is limited to unity-Lewis-number flames and, being expressed in terms of a mixture fraction coordinate, is not convenient in situations where the external fluid dynamical flow is not obvious *a priori*.

In this study, we derive a general formulation, not restricted to any particular configuration, for diffusion flames. The simplified equations are multi-dimensional and time-dependent and are expressed in terms of the physical coordinates. Furthermore, they allow for density variations as well as for two distinct and general Lewis numbers, one for the fuel and the other for the oxidant. The derivation is based on the assumption that the activation energy parameter is large and, as such, parallels the development of Linan's (1974) seminal work which thoroughly describes the structure of a planar diffusion flame in a counterflow with unity Lewis numbers. In this limit, the chemical reactions are all confined to a thin zone which, when viewed on the much larger diffusion scale, is a moving two-dimensional sheet. Although the structure of the thin reaction zone reduces in form to that analysed by Linan, the associated parameters that relate this structure to the external conditions on either side of the sheet are spatially and temporally dependent. These conditions are expressed as jumps for the temperature, mass fractions, velocity and pressure across the reaction sheet, and are sufficient for the determination of the external combustion field as well as the instantaneous shape of the reaction sheet. They include, in particular, expressions for the fuel and/or oxidant leakage through the reaction zone which, when excessive, lead to extinction. The formulation is therefore applicable to conditions extending from complete combustion down to extinction. Finally, we note that the discussion in this paper is limited to what Linan refers to as the 'diffusion-flame' or 'near-equilibrium' regime; the 'premixed-flame' regime, associated with a large leakage of one of the two reactants can be similarly discussed.

It should be mentioned that Lewis number effects on diffusion flames have been previously discussed for particular configurations. For example, Chung & Law (1983) discussed the structure of several one-dimensional flame configurations, Kim & Williams (1977) examined the extinction characteristics of a counterflow flame and Mills & Matalon (1997, 1998) analysed the structure and extinction characteristics of burner-generated spherical diffusion flames.

The large-activation-energy formulation that we derive is subsequently used to examine the occurrence and onset of diffusive-thermal instabilities in diffusion flames. Studies of intrinsic instabilities in flames have been predominantly concerned with premixed systems. A manifestation of an intrinsic instability is the spontaneous development of cellular structures, which is commonly observed in premixed flames. It is known that the competing effects of thermal and mass diffusivities play a central role in the development of cellular flames. One might therefore expect that they play a similar role in the stability of diffusion flames; however, very little has been done on the subject. Before giving a brief outline of our predictions, we first review the experimental evidence of cellular diffusion flames and provide an account of the relevant theoretical studies pertaining to stability issues.

The first known example of diffusive-thermal instability in diffusion flames is due to Garside & Jackson (1951, 1953). They observed that when a mixture of hydrogen and carbon dioxide, or hydrogen and nitrogen, was burnt in air, the surface of the

resulting jet diffusion flame often had a polyhedral structure. The surface of the flame in this case was formed of triangular cells in the shape of a polyhedron. The cells at the base of the flame were approximately 0.7 cm in width. The polyhedral flame was seen at relatively high flow rates and when the hydrogen was sufficiently diluted. Later, Dongworth & Melvin (1976) carried out experiments using a splitter-plate burner and the diffusion flame was formed with lean hydrogen–oxygen diluted in nitrogen. Under normal conditions the base of the diffusion flame, close to the burner partition, was straight. However, at sufficiently high flow velocities, and when the hydrogen concentration was substantially reduced, a cellular flame base was observed. The cells were about 1 cm in length. The same behaviour was noticed when the nitrogen in the fuel stream was replaced by argon, but not when replaced by helium. Ishizuka & Tsuji (1981) have also reported a similar behaviour in counterflow diffusion flames when the hydrogen, in a hydrogen–oxygen flame, was diluted with nitrogen and argon but not with helium. At near-extinction conditions, stripes formed on the flame surface along the flow with a periodic structure in the unstrained cross-flow direction. The wavelength of this periodic structure was not reported. Perhaps the most elaborate study was the recent work of Chen, Mitchell & Ronney (1992), who employed a slot burner and examined the occurrence of cellular flames in a variety of fuels and diluents and for various mixture strengths. Their findings, consistent with the earlier studies, were tabulated in table 1 of their paper. They pointed out that, far from extinction, no mixture exhibited cellularity. Cellular flames were formed at near-extinction conditions, when the Lewis number of the more completely consumed reactant was sufficiently less than 1. Depending on the conditions, the observed cells were approximately 0.7–1.5 cm in length.

The onset of diffusive-thermal instabilities in premixed flames is well understood. A premixed system, removed from stoichiometry, depends primarily on a single Lewis number Le defined as the ratio of the thermal diffusivity of the mixture (determined by the abundant species in the mixture) to the mass diffusivity of the deficient species (the binary diffusion coefficient of the deficient reactant and the inert) in the mixture. Theory predicts (Sivashinsky 1977; Buckmaster & Ludford 1982) that when $Le \approx 1$, a premixed flame is stable to diffusive-thermal effects; instabilities develop only when Le either exceeds, or is below, a critical value.† A cellular instability is predicted when Le is sufficiently less than 1, and an instability associated with pulsations and/or the development of travelling waves along the flame front when Le is sufficiently larger than 1. It is therefore expected that the disparity between the diffusivities of fuel and oxidant on one hand, and between mass and heat on the other, plays a similar role in the spontaneous development of cells in diffusion flames. Although physical arguments along these lines were suggested in some of the previously listed references, a comprehensive theory has not been offered.

A complete theory on the stability of diffusion flames appears more complex than that of premixed flames. First, for a diffusion flame there are two effective Lewis numbers – one associated with the fuel, L_F, and the other with the oxidant, L_X. The observations reported in Chen *et al.* (1992) suggest that, in general, the existence of cellular flames is not restricted to $L_F = L_X$. Second, unlike premixed flames, the structure of a diffusion flame varies with the Damköhler number D – the ratio of the

† The hydrodynamic instability, or Darrieus–Landau instability, resulting from the gas thermal expansion is always present in premixed flames. The hydrodynamic instability, however, is relatively weak for disturbances of long wavelengths, so that its influence can be minimized by restricting the lateral size of the experimental apparatus.

diffusion time to the chemical-reaction time. For very large D complete combustion occurs in an infinitesimally thin reaction sheet as envisaged by Burke & Schumann (1928), but for moderate values of D combustion is incomplete and there is leakage of one or both reactants through the reaction zone. Furthermore, combustion is not possible when D is too low; it is known that extinction occurs at $D = D_{\rm ex}$ where an excessive leakage of one or both reactants develops. As the experiments suggest, cellular flames occur mostly at near-extinction conditions, i.e. when D is sufficiently near $D_{\rm ex}$. The Damköhler number is therefore an important parameter that controls, among other things, the onset of cellularity. Third, unlike a premixed flame there is no characteristic speed associated with a diffusion flame. An observer moving with the premixed front always sees a mass flux of fuel and oxidant approaching from the unburned side of the flame. In contrast, the net mass flux through a diffusion flame, as seen by an observer located at the reaction front, can be directed from the fuel side or from the oxidant side. Observations seem to imply that a relation exists between the direction of the mass flux through the reaction sheet and the occurrence of cellular flames. All these considerations must therefore be incorporated in a complete theory.

While no comprehensive, theoretical study of diffusion flame stability exists, fragments appear in the literature. Studies by Peters (1978), Matalon & Ludford (1980) and Buckmaster, Nachman & Taliaferro (1983), concerned with the multiplicity of solutions, examined the response of a diffusion flame to one-dimensional disturbances while assuming unity Lewis numbers. Kirkby & Schmitz (1966), Fischer *et al.* (1994) and Cheatham & Matalon (1996*a*, *b*) were concerned with the onset of oscillations in diffusion flames. The only theoretical work that addresses the occurrence of cellular flames is that of Kim, Williams & Ronney (1996) and Kim (1997). They performed a linear stability analysis of a plane flame in the limit of large activation energy ($\theta \gg 1$) and for the case of equal Lewis numbers, $L_F = L_X$. It was shown in Kim *et al.* (1996) that, for Lewis numbers less than 1 and for wavelengths comparable to the diffusion length, flame instability exists for $D_{\rm ex} < D < D_c$, with the critical D_c identifying the onset of instability. The growth rate was found to increase indefinitely with the wavenumber k. Stabilization of small wavelengths occurs on a much shorter scale, comparable to the reaction zone thickness, with disturbances evolving on the corresponding fast time scale. A dispersion relation was then written by constructing a 'composite expansion' from the results corresponding to these two length scales, from which the transverse cell size $\ell_{\rm T}$ was estimated. It was found that $\ell_{\rm T} \sim (2\pi\ell_D)\theta^{-1/3}$ where ℓ_D is the diffusion length defined as the ratio of the thermal diffusivity of the mixture to a characteristic velocity. Since these results are based on the asymptotic limit of large θ, the onset of instability would therefore be associated with the development of relatively small cells $\sim \theta^{-1/3}$ in size. The analysis of Kim (1997) was motivated by the desire to identify a distinguished limit that leads to results that are free of the shortcomings of Kim *et al.* (1996). It was shown that $O(1)$ cell sizes result when the common Lewis number Le is close to 1, namely $Le - 1 = O(\theta^{-1})$. In this case the onset of instability occurs for $D = D^*$ with D^* close to but slightly larger than D_c; more specifically with $D^* - D_c = O(\theta^{-2})$.

In this paper we are also concerned with the stability of diffusion flames and, in particular, with the onset of cellular flames. The analysis is based on the general formulation that we derive in the first part of the paper and summarized in § 4. For simplicity, we examine the stability of a one-dimensional diffusion flame with one of the reactants (the fuel in the chosen set-up) transported, by means of convection and diffusion, towards the other, which diffuses against the stream from some finite location (see figure 7, below). Other configurations, such as a counterflow diffusion

flame, can be similarly analysed; their solution, however, involves special functions that render the analysis more complicated. The one-dimensional flame considered in Kim *et al.* (1996) and Kim (1997) is somewhat different from ours; there the reactants are supplied at two porous plates held a fixed distance from each other, and thus the problem involves the additional separation distance as a parameter. Apart from the different boundary conditions, whose effect on the stability results is not clear, both studies assume constant density and a large-activation-energy parameter. However, the derivations of the dispersion relations are different, as is the methodology used to obtain solutions of the respective dispersion relations. The methodology adopted by Kim *et al.* (1996) requires simultaneously solving a differential equation describing the reaction zone structure, numerically. In the present approach, the structure of the reaction zone is integrated once and for all, and the relevant information is contained in the correlations that we have constructed as part of our general model. The simplicity and straightforward manner by which the dispersion relation is analysed permits obtaining results over a wide range of parameters, as we do. Additional discussion of the analysis of the dispersion relation may be found in Cheatham's (1997) dissertation.

Our results show that, unlike Kim *et al.* (1996) and Kim (1997), the onset of cellular flames occurs at $D = D^*$ with D^* larger than D_c, and $D^* - D_c = O(1)$. Thus, the range of instability extends to $D_{\mathrm{ex}} < D < D^*$ with the critical D^* depending on all other physico-chemical parameters. The wavelength associated with the maximum growth rate at marginal stability, indicative of the dimension of the cells, is comparable to the diffusion length such that $\ell_{\mathrm{T}} \sim 2\pi\ell_D$. The predicted cell size, therefore, compares well with the experimental data. We show, in particular, that an instability results when the reactant supplied in the feed stream is the more completely consumed reactant and the corresponding Lewis number is below some critical value. Thus, when fuel is convected against an oxidant ambient and, as a result of the prevailing conditions the fuel is the more completely consumed reactant, cellular flames will occur when $L_F < L_F^*$. The critical Lewis number L_F^* depends on L_X as well as on the initial mixture strength ϕ. Cellular flames in this case are more likely to occur in more diluted, or 'leaner' flames. Stability curves that map the Lewis-number parameter plane, i.e. L_F versus L_X, are drawn for different values of the parameter ϕ and the Damköhler number D. For the inverted flame, with a net mass flux directed from the oxidant to the fuel side, the role of fuel and oxidant must be interchanged. Instability in this case is predicted for 'richer' flames, provided $L_X < L_X^*$. However, oxidants with such low Lewis numbers are seldom found, which explains why cellular flames under such conditions are rarely observed. Finally we note that although the present discussion has been limited to the onset of cellular flames, the dispersion relation that we have derived exhibits other forms of instabilities, such as pulsating flames and travelling wave solutions; these will be discussed in future publications.

The paper is made up of two parts and organized as follows. In the first part we present the governing equations, the general structure of the reaction zone in its intrinsic coordinates, and a summary of the simplified model. The second part is devoted to flame stability and includes the description of the basic plane flame solution, the derivation of the dispersion relation and its analysis as it pertains to the onset of cellular flames.

2. Governing equations

We consider a gaseous combustion system in which the fuel and oxidant, initially separated, are immersed in an inert gas that appears in abundance. For convenience,

we assume that far to the left the mixture contains fuel but no oxidant, whereas far to the right it contains oxidant but no fuel. The chemical activity that occurs in the mixing layer is modelled by a one-step global irreversible reaction of the form

$$v_F F + v_X X \rightarrow \text{ Products } + \{Q\}$$

where v_i is the stoichiometric coefficient of species i, with the subscripts F, X identifying the fuel and oxidant, respectively, and where Q is the total chemical heat release. The chemical reaction rate is assumed to be of Arrhenius type with an overall activation energy E and a pre-exponential factor $\mathscr{B}$. The reaction rate is therefore of the form

$$\tilde{\omega} = \mathscr{B}\left(\frac{\tilde{\rho}\tilde{Y}}{W_F}\right)\left(\frac{\tilde{\rho}\tilde{X}}{W_X}\right)\mathrm{e}^{-E/R^o\tilde{T}} \tag{2.1}$$

with $\tilde{\rho}$, $\tilde{T}$ the density and temperature of the mixture, W_i the molecular weight of species i and R^o the universal gas constant. The tilde denotes dimensional quantities.

Letting $\tilde{\boldsymbol{v}}$ be the velocity field, $\tilde{p}$ the pressure and $\tilde{Y}, \tilde{X}$ the fuel and oxidant mass fractions, the equations describing the mixing and chemical reaction processes are

$$\frac{\partial\tilde{\rho}}{\partial\tilde{t}} + \tilde{\nabla}\cdot\tilde{\rho}\tilde{\boldsymbol{v}} = 0, \tag{2.2}$$

$$\tilde{\rho}\frac{\mathrm{D}\tilde{\boldsymbol{v}}}{\mathrm{D}\tilde{t}} = -\tilde{\nabla}\tilde{p} + \tilde{\rho}\boldsymbol{g} + \mu\{\tilde{\nabla}^2\tilde{\boldsymbol{v}} + \tfrac{1}{3}\tilde{\nabla}(\tilde{\nabla}\cdot\tilde{\boldsymbol{v}})\}, \tag{2.3}$$

$$\tilde{\rho}c_p\frac{\mathrm{D}\tilde{T}}{\mathrm{D}\tilde{t}} - \tilde{\nabla}\cdot(\lambda\tilde{\nabla}\tilde{T}) = Q\tilde{\omega}, \tag{2.4}$$

$$\tilde{\rho}\frac{\mathrm{D}\tilde{Y}}{\mathrm{D}\tilde{t}} - \tilde{\nabla}\cdot(\tilde{\rho}\mathscr{D}_F\tilde{\nabla}\tilde{Y}) = -v_F W_F\,\tilde{\omega}, \tag{2.5}$$

$$\tilde{\rho}\frac{\mathrm{D}\tilde{X}}{\mathrm{D}\tilde{t}} - \tilde{\nabla}\cdot(\tilde{\rho}\mathscr{D}_X\tilde{\nabla}\tilde{X}) = -v_X W_X\,\tilde{\omega}. \tag{2.6}$$

They represent, respectively, mass, momentum and energy conservation of the whole mixture, and mass balances for the fuel and oxidant. The operator $\mathrm{D}/\mathrm{D}\tilde{t} \equiv \partial/\partial\tilde{t} + \tilde{\boldsymbol{v}}\cdot\tilde{\nabla}$ is the convective derivative and $\boldsymbol{g}$ is the gravitational force (per unit mass). The mixture's properties, i.e. the viscosity μ, the thermal conductivity λ and the specific heat (at constant pressure) c_p, are all assumed constant. The molecular diffusivities for the fuel and oxidant (relative to the inert gas) are assumed temperature dependent such that $\tilde{\rho}\mathscr{D}_i$ are constants. The energy equation (2.4) has been written for conditions in which the burning takes place in open space with representative velocities much smaller than the speed of sound. For such flows the spatial variations in pressure, which balance the change in momentum described in (2.3), are small compared to the pressure itself. Consequently, the rate of change of the kinetic energy of the mixture and the work associated with these small changes in pressure are negligible. The small pressure variations may also be neglected in the equation of state, which now reads

$$\tilde{P}_c = \tilde{\rho}R^o\tilde{T}/\overline{W} \tag{2.7}$$

where $\tilde{P}_c$ is the constant ambient pressure and $\overline{W}$ the molecular weight of the mixture. In general $\overline{W}$ depends on the mixture's composition and, therefore, varies across the combustion field; but for simplicity we shall take it as a constant.

Equations (2.2)–(2.7) must be supplemented by appropriate initial and boundary conditions reflecting the way in which the fuel and oxidant are supplied and the fact

that they are initially separated and may be provided at different temperatures. These conditions introduce a characteristic velocity U and an initial fuel concentration $\tilde{Y}_{-\infty}$. We normalize the mass fractions of the fuel and oxidant with $\tilde{Y}_{-\infty}$ and $\nu\tilde{Y}_{-\infty}$ respectively, where $\nu = \nu_X W_X/\nu_F W_F$ is the mass-weighted stoichiometric coefficient ratio. The ambient pressure P_c is used as a unit of pressure and q/c_p, with $q = Q\tilde{Y}_{-\infty}/\nu_F W_F$ the heat released per unit mass of fuel supplied, as a unit of temperature. Consequently, the characteristic density is $\tilde{\rho}_c = P_c\overline{W}c_p/qR^o$. The small pressure variations in the momentum equation are thus proportional to the square of the representative Mach number, namely $\sim P_c\tilde{\rho}_c^{-1}/U^2$. Finally the diffusion length $\ell_D \equiv \lambda/\tilde{\rho}_c c_p U$ is used as a unit of length and ℓ_D/U as a unit of time.

The characteristic chemical time is of the order of the inverse of the reaction constant $\sim \mathscr{B}\exp(-E/R^o\tilde{T}_a)$ where $\tilde{T}_a$ is the 'adiabatic flame temperature' corresponding to complete consumption of reactants.† Hence the ratio of the residence time $\sim \lambda/\tilde{\rho}_a c_p U^2$, where $\tilde{\rho}_a$ is the density corresponding to the state at which $\tilde{T} = \tilde{T}_a$, to the chemical time defines a Damköhler number which can be properly written in the form‡

$$D = \frac{\lambda}{\tilde{\rho}_a c_p U^2}\left(\frac{R^o\tilde{T}_a}{E}\right)^3 \frac{\nu_X c_p \overline{W}}{qR^o W_F}\mathscr{B}\,\tilde{Y}_{-\infty}\,\mathrm{e}^{-E/R\tilde{T}_a}. \tag{2.8}$$

The chemical reaction rate, in dimensionless form, becomes

$$\omega = D\,T_a^2\theta^3\rho^2 XY\exp\left\{\frac{\theta(T-T_a)}{T/T_a}\right\} \tag{2.9}$$

with $\theta = qE/c_pR^o\tilde{T}_a^2$ the activation-energy parameter, or the Zeldovich number. Hereafter the symbols without a tilde denote the same quantity but in dimensionless form. The dimensionless governing equations become

$$\frac{\partial\rho}{\partial t} + \nabla\cdot\rho\boldsymbol{v} = 0, \tag{2.10}$$

$$\rho\frac{\mathrm{D}\boldsymbol{v}}{\mathrm{D}t} = -\nabla p + Fr^{-1}\rho\boldsymbol{e}_g + Pr\{\nabla^2\boldsymbol{v} + \tfrac{1}{3}\nabla(\nabla\cdot\boldsymbol{v})\}, \tag{2.11}$$

$$\rho\frac{\mathrm{D}T}{\mathrm{D}t} - \nabla^2 T = \omega, \tag{2.12}$$

$$\rho\frac{\mathrm{D}Y}{\mathrm{D}t} - \frac{1}{L_F}\nabla^2 Y = -\omega, \tag{2.13}$$

$$\rho\frac{\mathrm{D}X}{\mathrm{D}t} - \frac{1}{L_X}\nabla^2 X = -\omega, \tag{2.14}$$

$$\rho T = 1, \tag{2.15}$$

with $\boldsymbol{e}_g$ a unit vector in the direction of gravity. The remaining parameters that

† In general, $\tilde{T}_a$ depends on the supply conditions and on the way in which the fuel and oxidant are brought together; this in contrast to the more clearly defined 'adiabatic flame temperature' of a premixed combustible mixture.

‡ This form assumes a distinguished limit that relates the magnitudes of the Damköhler number and the activation energy which, as will become clearer, is the appropriate one for the asymptotic treatment considered below. This limit covers the range of Damköhler numbers from an infinitely fast rate (Burke–Schumann limit) down to extinction. A different distinguished limit is needed to cover the range of Damköhler numbers from frozen conditions, or small D, up to ignition.

appear in these equations are the Froude number $Fr = U^2/|\boldsymbol{g}|\ell_D$, the Prandtl number $Pr = \mu c_p/\lambda$, and the Lewis numbers $L_F = \lambda/c_p\tilde{\rho}\mathscr{D}_F$ and $L_X = \lambda/c_p\tilde{\rho}\mathscr{D}_X$.

In the following section we derive a general formulation, which is appropriate for large-activation-energy chemical reactions. We shall therefore exploit the limit of $\theta \gg 1$ allowing the Damköhler number D, defined as in (2.8), to vary independently. As we shall see, for a flame to exist D must be limited from below, so that $D_{\text{ex}} < D < \infty$ with D_{ex} corresponding to flame extinction.

3. The reaction zone structure

When the activation-energy parameter θ is large, the chemical activity is confined to a thin zone which reduces, in the limit $\theta \to \infty$, to a surface. This surface, referred to as the *reaction sheet*, is determined at any given instant by the function

$$F(\boldsymbol{x}, t) = 0. \tag{3.1}$$

The reaction sheet separates a region of primarily fuel from a region of primarily oxidant. We shall identify the *fuel region* as the region where $F < 0$ and the *oxidant region* as the region where $F > 0$. Furthermore, we shall assume that in the fuel region $X = o(1)$ and in the oxidant region $Y = o(1)$. Thus, to leading order, both reactants vanish at the reaction sheet and the temperature along the sheet is the adiabatic flame temperature T_a, assumed constant.† This is the fast chemistry, or Burke–Schumann limit of complete combustion (Burke & Schumann 1928). Spatial and temporal variations in temperature along the reaction sheet are thus within $O(\theta^{-1})$ of T_a.

On either side of the reaction sheet the chemical reaction rate is exponentially small (since $T < T_a$), and therefore negligible. If the solution in these 'outer' regions is expanded in power series of θ^{-1}, i.e. in the form

$$\left.\begin{aligned}
\rho &\sim \rho_0(\boldsymbol{x}, t) + \theta^{-1}\rho_1(\boldsymbol{x},t) + \theta^{-2}\rho_2(\boldsymbol{x}, t) + \cdots,\\
\boldsymbol{v} &\sim \boldsymbol{v}_0(\boldsymbol{x}, t) + \theta^{-1}\boldsymbol{v}_1(\boldsymbol{x},t) + \theta^{-2}\,\boldsymbol{v}_2(\boldsymbol{x}, t) + \cdots,\\
p &\sim p_0(\boldsymbol{x}, t) + \theta^{-1}p_1(\boldsymbol{x}, t) + \theta^{-2}p_2(\boldsymbol{x}, t) + \cdots,\\
T &\sim T_0(\boldsymbol{x}, t) + \theta^{-1}T_1(\boldsymbol{x}, t) + \theta^{-2}T_2(\boldsymbol{x}, t) + \cdots,\\
Y &\sim Y_0(\boldsymbol{x}, t) + \theta^{-1}Y_1(\boldsymbol{x}, t) + \theta^{-2}Y_2(\boldsymbol{x}, t) + \cdots,\\
X &\sim X_0(\boldsymbol{x}, t) + \theta^{-1}X_1(\boldsymbol{x}, t) + \theta^{-2}X_2(\boldsymbol{x}, t) + \cdots,
\end{aligned}\right\} \tag{3.2}$$

then $Y_0 \equiv 0$ for $F > 0$ and $X_0 \equiv 0$ for $F < 0$. The remaining variables are determined by solving the governing equations (2.10)–(2.15) with the reaction rate set to zero. Appropriate conditions must then be added to the outer variables, relating their values on both sides of the interface. These jump relationships are derived from analysing the reaction zone structure, as we do next.

3.1. *Intrinsic coordinates*

Let $\boldsymbol{r}$ be the position vector of a point P in space, measured at time t, with respect to a fixed coordinate system; hence

$$\boldsymbol{r} = \boldsymbol{r}(\boldsymbol{x}, t). \tag{3.3}$$

† This does not necessarily imply that the reaction sheet needs to be planar or nearly planar. For example, under quite general conditions it can be shown that for unity Lewis numbers, the temperature T_a along the reaction sheet, whatever its shape, is a constant. See the discussion in § 3.4 and the determination of T_a.

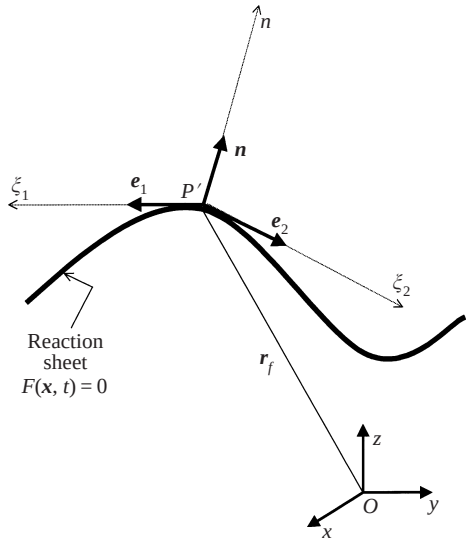

FIGURE 1. The curvilinear coordinates.

The position of the point P may also be described by means of its distance n from the reaction sheet and the position vector $\boldsymbol{r}_f$ of the projection of P on the reaction sheet. We denote the unit normal to the reaction sheet by $\boldsymbol{n}$ and use the intrinsic surface coordinates (ξ_1, ξ_2) aligned with the principal directions of curvature at each point of the reaction sheet to parameterize the surface (see figure 1). Thus $\boldsymbol{r}_f = \boldsymbol{r}_f(\xi_1, \xi_2, t)$ and

$$\boldsymbol{r} = \boldsymbol{r}_f(\xi_1, \xi_2, t) + n\,\boldsymbol{n}(\xi_1, \xi_2, t), \tag{3.4}$$

so that (ξ_1, ξ_2, n) may be taken as curvilinear coordinates of P. To avoid unnecessary additional notation, we denote the time variable in the moving coordinate system also by t. Let $\boldsymbol{e}_1$ and $\boldsymbol{e}_2$ denote unit vectors tangential to the parametric curves $\xi_2 = \text{const.}$ and $\xi_1 = \text{const.}$, respectively, given by

$$\boldsymbol{e}_1 = \frac{1}{a_1}\frac{\partial \boldsymbol{r}_f}{\partial \xi_1}, \qquad \boldsymbol{e}_2 = \frac{1}{a_2}\frac{\partial \boldsymbol{r}_f}{\partial \xi_2} \tag{3.5}$$

with $a_i = |\partial \boldsymbol{r}_f / \partial \xi_i|$. Then $\boldsymbol{e}_1, \boldsymbol{e}_2$ and $\boldsymbol{n} = \boldsymbol{e}_1 \times \boldsymbol{e}_2$ form an orthogonal triad of unit vectors. The orientation of the curvilinear coordinates is chosen such that $\boldsymbol{n}$ points in the direction of the oxidant region, so that $n > 0$ corresponds to $F > 0$, and $n < 0$ corresponds to $F < 0$. The transformation (3.4) may be used to relate the variables (x, y, z) in the fixed frame to the variables (ξ_1, ξ_2, n) in the moving frame. Standard results from differential geometry (e.g. Weatherburn 1947), provide the *scale factors*

$$h_1 = a_1(1 - n\kappa_1), \quad h_2 = a_2(1 - n\kappa_2), \quad h_3 = 1$$

used in the computation of the vector differential operators. Here κ_1 and κ_2 are the principal curvatures of the reaction sheet surface in the ξ_1- and ξ_2-directions, respectively. Thus, $\kappa = (\kappa_1 + \kappa_2) = -\nabla \cdot \boldsymbol{n}$ (evaluated at $n = 0$) is twice the mean curvature of the surface. The gradient operator now takes the form

$$\nabla = \boldsymbol{e}_1 \frac{1}{h_1}\frac{\partial}{\partial \xi_1} + \boldsymbol{e}_2 \frac{1}{h_2}\frac{\partial}{\partial \xi_2} + \boldsymbol{n}\frac{\partial}{\partial n} \tag{3.6}$$

and the divergence, of a vector $\boldsymbol{u}$ say, is

$$\nabla \cdot \boldsymbol{u} = \frac{1}{h_1 h_2}\left[\frac{\partial}{\partial \xi_1}(h_2 u_1) + \frac{\partial}{\partial \xi_2}(h_1 u_2) + \frac{\partial}{\partial n}(h_1 h_2 u_3)\right] \tag{3.7}$$

where u_1, u_2, u_3 are the components of $\boldsymbol{u}$ in the directions $\boldsymbol{e}_1, \boldsymbol{e}_2$ and $\boldsymbol{n}$, respectively. All other vector operations can be deduced from these in a straightforward manner and appear in standard textbooks. Useful references, that utilize similar curvilinear coordinates are, for example, Rosenhead (1963); Yao & Stewart (1996) and Ida & Miksis (1998).

The time derivative in the fixed coordinates is related to that in the frame attached to the reaction sheet by making the change

$$\frac{\partial}{\partial t} \to \frac{\partial}{\partial t} + \frac{\partial \xi_1}{\partial t}\frac{\partial}{\partial \xi_1} + \frac{\partial \xi_2}{\partial t}\frac{\partial}{\partial \xi_2} - V_f \frac{\partial}{\partial n},$$

where $V_f \equiv -\partial n/\partial t$ is the velocity of the surface back along the normal and $\partial \xi_i/\partial t$ is proportional to the instantaneous rate of change of the arclength in the ξ_i-direction. Note that V_f is considered positive when the reaction sheet moves towards the fuel region.

To examine the internal structure of the reaction zone, we introduce the stretching transformation $n = \eta/\theta$ along with the 'inner' expansions

$$\left.\begin{aligned}
\boldsymbol{v} &\sim \boldsymbol{V}_0(\xi_1, \xi_2, \eta, t) + \theta^{-1}\boldsymbol{V}_1(\xi_1, \xi_2, \eta, t) + \theta^{-2}\boldsymbol{V}_2(\xi_1, \xi_2, \eta, t) + \cdots,\\
p &\sim P_0(\xi_1, \xi_2, \eta, t) + \theta^{-1}P_1(\xi_1, \xi_2, \eta, t) + \theta^{-2}P_2(\xi_1, \xi_2, \eta, t) + \cdots,\\
T &\sim T_a + \theta^{-1}\tau_1(\xi_1, \xi_2, \eta, t) + \theta^{-2}\tau_2(\xi_1, \xi_2, \eta, t) + \cdots,\\
\rho &\sim \rho_a + \theta^{-1}\varrho_1(\xi_1, \xi_2, \eta, t) + \theta^{-2}\varrho_2(\xi_1, \xi_2, \eta, t) + \cdots,\\
Y &\sim \theta^{-1}y_1(\xi_1, \xi_2, \eta, t) + \theta^{-2}y_2(\xi_1, \xi_2, \eta, t)\cdots,\\
X &\sim \theta^{-1}x_1(\xi_1, \xi_2, \eta, t) + \theta^{-2}x_2(\xi_1, \xi_2, \eta, t)\cdots,
\end{aligned}\right\} \tag{3.8}$$

where, as assumed, the fuel and oxidant mass fractions are $O(\theta^{-1})$ and the temperature is within $O(\theta^{-1})$ of the adiabatic flame temperature T_a. The equation of state (2.15) implies

$$\rho_a = 1/T_a, \quad \varrho_1 = -\rho_a^2\tau_1, \quad \varrho_2 = -\rho_a^2\tau_2 + \rho_a^3\tau_1^2. \tag{3.9}$$

(Note the slightly different symbol used for the inner variables representing the density). Introducing the stretching transformation and the inner expansions (3.8) in the governing equations written in terms of the intrinsic coordinates, then collecting like powers of θ, we obtain a series of systems of equations which we must consider in turn. The solutions of these equations must be matched with the outer expansions as $\eta \to \pm\infty$. The matching conditions are simply obtained by expanding the outer expansions near $n = 0^{\pm}$. For example, for the pressure we have

$$p \sim p_0^{\pm} + \theta^{-1}\left\{\left.\frac{\partial p_0}{\partial n}\right|^{\pm}\eta + p_1^{\pm}\right\} + \theta^{-2}\left\{\left.\frac{1}{2}\frac{\partial^2 p_0}{\partial n^2}\right|^{\pm}\eta^2 + \left.\frac{\partial p_1}{\partial n}\right|^{\pm}\eta + p_2^{\pm}\right\} + \cdots,$$

where the superscript $\pm$ denotes that the quantity is to be evaluated at $n = 0^+$ or $n = 0^-$, respectively, and therefore depends on ξ_1, ξ_2 and t only. This implies that

$$P_0 \sim p_0^{\pm}, \quad P_1 \sim \left.\frac{\partial p_0}{\partial n}\right|^{\pm}\eta + p_1^{\pm}, \quad P_2 \sim \left.\frac{1}{2}\frac{\partial^2 p_0}{\partial n^2}\right|^{\pm}\eta^2 + \left.\frac{\partial p_1}{\partial n}\right|^{\pm}\eta + p_2^{\pm}$$

as $\eta \to \pm\infty$, respectively. Similarly we can write the matching conditions for all other variables. Finally, we note that in writing the inner expansions (3.8), we have anticipated that, to leading order, all state variables are continuous across the reaction sheet, namely

$$[\rho_0] = [T_0] = [Y_0] = [X_0] = 0, \tag{3.10}$$

where the square bracket denotes the jump in the quantity, for example $[\rho_0] = \rho_0^+ - \rho_0^-$.

For simplicity of discussion the equations of conservation of mass and momentum are considered first, to be followed by an analysis of the equations for the temperature and mass fractions.

3.2. *Mass and momentum*

It is convenient to express the velocities in the form $\boldsymbol{V}_i = U_i\boldsymbol{e}_1 + V_i\boldsymbol{e}_2 + W_i\boldsymbol{n}$ for the inner variables and, equivalently, $\boldsymbol{v}_i = u_i\boldsymbol{e}_1 + v_i\boldsymbol{e}_2 + w_i\boldsymbol{n}$ for the outer variables. To leading order, we find that

$$\frac{\partial W_0}{\partial \eta} = 0, \qquad \frac{\partial^2 \boldsymbol{V}_0}{\partial \eta^2} = 0$$

which implies that $\boldsymbol{V}_0 = \boldsymbol{V}_0(\xi_1, \xi_2, t) = \boldsymbol{v}_0^{\pm}$. Thus, all velocity components are continuous across the reaction sheet, namely

$$[\boldsymbol{v}_0] = 0. \tag{3.11}$$

In particular $[\rho_0(w_0 - V_f)] = 0$, which implies that the mass flux across the reaction zone is conserved. We shall denote by m the mass flux normal and relative to the reaction sheet, so that $m \equiv \rho(w - V_f)$. Consequently, we introduce the (outer) expansion $m = m_0 + \theta^{-1}m_1 + \theta^{-2}m_2 + \cdots$, with the m_i obviously related to the ρ_i and w_i. The corresponding inner expansion is

$$m = M_0(\xi_1, \xi_2, t) + \theta^{-1}M_1(\xi_1, \xi_2, \eta, t) + \theta^{-2}M_2(\xi_1, \xi_2, \eta, t) + \cdots,$$

where we have used (3.11) in indicating that M_0, the leading term of the normal mass flux at the reaction sheet, is independent of η.

To $O(\theta^{-1})$ the equations reduce to

$$(W_0 - V_f)\frac{\partial \varrho_1}{\partial \eta} + \rho_a \frac{\partial W_1}{\partial \eta} = -\frac{\rho_a}{a_1 a_2}\left\{\frac{\partial}{\partial \xi_1}(a_2 U_0) + \frac{\partial}{\partial \xi_2}(a_1 V_0) - \kappa a_1 a_2 W_0\right\}, \tag{3.12}$$

$$\frac{\partial^2 U_1}{\partial \eta^2} = \frac{\partial^2 V_1}{\partial \eta^2} = 0, \qquad \frac{\partial P_0}{\partial \eta} - \tfrac{4}{3}Pr\frac{\partial^2 W_1}{\partial \eta^2} = 0, \tag{3.13}$$

and must satisfy the matching conditions $\boldsymbol{V}_1 \sim \eta(\partial \boldsymbol{v}_0/\partial n)^{\pm} + \boldsymbol{v}_1^{\pm}$ and $\varrho_1 \sim \eta(\partial \rho_0/\partial n)^{\pm} + \rho_1^{\pm}$ as $\eta \to \pm\infty$. The right-hand side of (3.12) does not depend on η so that, when evaluated across the reaction zone, we obtain the jump relation

$$\rho_0\left[\frac{\partial w_0}{\partial n}\right] + (w_0 - V_f)\left[\frac{\partial \rho_0}{\partial n}\right] = 0 \tag{3.14}$$

or equivalently

$$\left[\frac{\partial m_0}{\partial n}\right] = 0. \tag{3.15}$$

Integrating (3.12) once yields

$$\rho_a W_1 + (W_0 - V_f)\varrho_1 + \frac{\rho_a}{a_1 a_2}\left(\frac{\partial}{\partial \xi_1}(a_2 U_0) + \frac{\partial}{\partial \xi_2}(a_1 V_0) - \kappa a_1 a_2 W_0\right)\eta = c(\xi_1, \xi_2, t) \tag{3.16}$$

with $c(\xi_1, \xi_2, t)$ a constant of integration. Applying the matching conditions as $\eta \to \pm\infty$ we find that

$$\eta\left\{(w_0^{\pm} - V_f)\frac{\partial \rho_0^{\pm}}{\partial n} + \rho_0^{\pm}\frac{\partial w_0^{\pm}}{\partial n} + \frac{1}{a_1 a_2}\left(\frac{\partial}{\partial \xi_1}(a_2 \rho_0^{\pm} u_0^{\pm}) + \frac{\partial}{\partial \xi_2}(a_1 \rho_0^{\pm} v_0^{\pm})\right) - \kappa \rho_0^{\pm} w_0^{\pm}\right\}$$
$$+(w_0^{\pm} - V_f)\rho_1^{\pm} + \rho_a w_1^{\pm} = c.$$

The expression in the curly bracket, which is merely the continuity equation evaluated at $n = 0^{\pm}$, vanishes identically. The remaining part yields

$$[m_1] \equiv [\rho_0 w_1 + \rho_1(w_0 - V_f)] = 0 \tag{3.17}$$

and determines $c(\xi_1, \xi_2, t) = m_1^-$ (or equivalently m_1^+). Hence the variations in the normal velocity component across the reaction zone are calculated from (3.16). The remaining equations (3.13) imply that

$$\left[\frac{\partial u_0}{\partial n}\right] = \left[\frac{\partial v_0}{\partial n}\right] = 0, \qquad [p_0] - \tfrac{4}{3}Pr\left[\frac{\partial w_0}{\partial n}\right] = 0, \tag{3.18}$$

$$[u_1] = [v_1] = 0, \tag{3.19}$$

and also provide the expression

$$\int_{-\infty}^{\infty} P_0(\eta)\,\mathrm{d}\eta = \lim_{\eta\to\infty}(p_0^+ \eta) - \lim_{\eta\to-\infty}(p_0^- \eta) + \tfrac{4}{3}Pr[w_1] \tag{3.20}$$

which will be needed later.

To complete the conditions needed to solve the outer system to $O(1/\theta)$, the equations must be taken to the next order. Now, the continuity equation takes the form

$$\frac{\partial \varrho_1}{\partial t} + \frac{\partial \xi_1}{\partial t}\frac{\partial \varrho_1}{\partial \xi_1} + \frac{\partial \xi_2}{\partial t}\frac{\partial \varrho_1}{\partial \xi_2} + \frac{\partial M_2}{\partial \eta} - \kappa(\rho_a W_1 + \varrho_1 W_0)$$
$$+\left\{\frac{\kappa}{a_1 a_2}\left(\frac{\partial}{\partial \xi_1}(a_2 U_0) + \frac{\partial}{\partial \xi_2}(a_1 V_0)\right)\right.$$
$$\left. - \frac{1}{a_1 a_2}\left(\frac{\partial}{\partial \xi_1}(a_2 \kappa_2 U_0) + \frac{\partial}{\partial \xi_2}(a_1 \kappa_1 V_0)\right) + (2\kappa_1\kappa_2 - \kappa^2)W_0\right\}\rho_a \eta$$
$$+\frac{1}{a_1 a_2}\left\{\frac{\partial}{\partial \xi_1}(\rho_a a_2 U_1 + \varrho_1 a_2 U_0) + \frac{\partial}{\partial \xi_2}(\rho_a a_1 V_1 + \varrho_1 a_1 V_0)\right\} = 0.$$

When evaluated across the reaction zone and use is made of the matching conditions as $\eta \to \pm\infty$ one finds that the terms which have η as a common factor vanish identically. These terms consist merely of the continuity equation differentiated with

respect to n and evaluated at $n = 0^{\pm}$. The remaining terms yield

$$\left[\frac{\partial m_1}{\partial n}\right] = \kappa V_f[\rho_1] - \left[\frac{\partial \rho_1}{\partial t} + \frac{\partial \xi_1}{\partial t}\frac{\partial \rho_1}{\partial \xi_1} + \frac{\partial \xi_2}{\partial t}\frac{\partial \rho_1}{\partial \xi_2}\right] - \frac{1}{a_1 a_2}\left[\frac{\partial}{\partial \xi_1}(a_2\rho_0 u_1 + a_2\rho_1 u_0) + \frac{\partial}{\partial \xi_2}(a_1\rho_0 v_1 + a_1\rho_1 v_0)\right]. \tag{3.21}$$

The momentum equation to $O(1/\theta)$ gives

$$\begin{aligned}
&\rho_a\left\{\frac{\partial U_0}{\partial t} + \frac{\partial \xi_1}{\partial t}\frac{\partial U_0}{\partial \xi_1} + \frac{\partial \xi_2}{\partial t}\frac{\partial U_0}{\partial \xi_2} + \frac{U_0}{a_1}\frac{\partial U_0}{\partial \xi_1} + \frac{V_0}{a_2}\frac{\partial U_0}{\partial \xi_2} - \frac{V_0^2}{a_1 a_2}\frac{\partial a_2}{\partial \xi_1} + \frac{U_0 V_0}{a_1 a_2}\frac{\partial a_1}{\partial \xi_2}\right\}\\
&+M_0\frac{\partial U_1}{\partial \eta} - \kappa_1 U_0 W_0 = -\frac{1}{a_1}\frac{\partial P_0}{\partial \xi_1}\\
&+\frac{Pr}{3}\left\{\frac{1}{a_1}\frac{\partial}{\partial \xi_1}\left(\frac{1}{a_1 a_2}\frac{\partial}{\partial \xi_1}(a_2 U_0) + \frac{1}{a_1 a_2}\frac{\partial}{\partial \xi_2}(a_1 V_0)\right) + \frac{1}{a_1}\frac{\partial^2 W_1}{\partial \xi_1 \partial \eta} - \frac{1}{a_1}\frac{\partial}{\partial \xi_1}(\kappa W_0)\right\}\\
&+Pr\left\{\frac{1}{a_1 a_2}\frac{\partial}{\partial \xi_1}\left(\frac{a_2}{a_1}\frac{\partial U_0}{\partial \xi_1}\right) + \frac{1}{a_1 a_2}\frac{\partial}{\partial \xi_2}\left(\frac{a_1}{a_2}\frac{\partial U_0}{\partial \xi_2}\right) + \frac{\partial^2 U_2}{\partial \eta^2} - \kappa\frac{\partial U_1}{\partial \eta} + (\kappa_1\kappa_2 - \kappa_1^2)U_0\right.\\
&-\frac{W_0}{a_1}\frac{\partial \kappa}{\partial \xi_1} - \frac{2\kappa_1}{a_1}\frac{\partial W_0}{\partial \xi_1} + \frac{V_0}{a_1}\frac{\partial}{\partial \xi_1}\left(\frac{1}{a_1 a_2}\frac{\partial a_1}{\partial \xi_2}\right) - \frac{V_0}{a_2}\frac{\partial}{\partial \xi_2}\left(\frac{1}{a_1 a_2}\frac{\partial a_2}{\partial \xi_1}\right)\\
&+\frac{U_0}{a_2}\frac{\partial}{\partial \xi_2}\left(\frac{1}{a_1 a_2}\frac{\partial a_1}{\partial \xi_2}\right) + \frac{U_0}{a_1}\frac{\partial}{\partial \xi_1}\left(\frac{1}{a_1 a_2}\frac{\partial a_2}{\partial \xi_1}\right) - \frac{1}{a_1 a_2^2}\frac{\partial a_2}{\partial \xi_1}\frac{\partial V_0}{\partial \xi_2} + \frac{1}{a_1^2 a_2}\frac{\partial a_1}{\partial \xi_2}\frac{\partial V_0}{\partial \xi_1}\\
&\left.+\frac{1}{a_1}\frac{\partial V_0}{\partial \xi_2}\frac{\partial}{\partial \xi_1}\left(\frac{1}{a_2}\right) - \frac{1}{a_2}\frac{\partial}{\partial \xi_2}\left(\frac{1}{a_1}\right)\frac{\partial V_0}{\partial \xi_1} + \frac{1}{a_1}\frac{\partial U_0}{\partial \xi_1}\frac{\partial}{\partial \xi_1}\left(\frac{1}{a_1}\right)\right\},
\end{aligned} \tag{3.22}$$

$$\begin{aligned}
&\rho_a\left\{\frac{\partial V_0}{\partial t} + \frac{\partial \xi_1}{\partial t}\frac{\partial V_0}{\partial \xi_1} + \frac{\partial \xi_2}{\partial t}\frac{\partial V_0}{\partial \xi_2} + \frac{U_0}{a_1}\frac{\partial V_0}{\partial \xi_1} + \frac{V_0}{a_2}\frac{\partial V_0}{\partial \xi_2} - \frac{U_0^2}{a_1 a_2}\frac{\partial a_1}{\partial \xi_2} + \frac{U_0 V_0}{a_1 a_2}\frac{\partial a_2}{\partial \xi_1}\right\}\\
&+M_0\frac{\partial V_1}{\partial \eta} - \kappa_2 V_0 W_0 = -\frac{1}{a_2}\frac{\partial P_0}{\partial \xi_2}\\
&+\frac{Pr}{3}\left\{\frac{1}{a_2}\frac{\partial}{\partial \xi_2}\left(\frac{1}{a_1 a_2}\frac{\partial}{\partial \xi_1}(a_2 U_0) + \frac{1}{a_1 a_2}\frac{\partial}{\partial \xi_2}(a_1 V_0)\right) + \frac{1}{a_2}\frac{\partial^2 W_1}{\partial \xi_2 \partial \eta} - \frac{1}{a_2}\frac{\partial}{\partial \xi_2}(\kappa W_0)\right\}\\
&+Pr\left\{\frac{1}{a_1 a_2}\frac{\partial}{\partial \xi_1}\left(\frac{a_2}{a_1}\frac{\partial V_0}{\partial \xi_1}\right) + \frac{1}{a_1 a_2}\frac{\partial}{\partial \xi_2}\left(\frac{a_1}{a_2}\frac{\partial V_0}{\partial \xi_2}\right) + \frac{\partial^2 V_2}{\partial \eta^2} - \kappa\frac{\partial V_1}{\partial \eta}\right.\\
&+(\kappa_1\kappa_2 - \kappa_2^2)V_0 - \frac{W_0}{a_2}\frac{\partial \kappa}{\partial \xi_2} - \frac{2\kappa_2}{a_2}\frac{\partial W_0}{\partial \xi_2} + \frac{U_0}{a_2}\frac{\partial}{\partial \xi_2}\left(\frac{1}{a_1 a_2}\frac{\partial a_2}{\partial \xi_1}\right) - \frac{U_0}{a_1}\frac{\partial}{\partial \xi_1}\left(\frac{1}{a_1 a_2}\frac{\partial a_1}{\partial \xi_2}\right)\\
&+\frac{V_0}{a_1}\frac{\partial}{\partial \xi_1}\left(\frac{1}{a_1 a_2}\frac{\partial a_2}{\partial \xi_1}\right) + \frac{V_0}{a_2}\frac{\partial}{\partial \xi_2}\left(\frac{1}{a_1 a_2}\frac{\partial a_1}{\partial \xi_2}\right) - \frac{1}{a_1^2 a_2}\frac{\partial a_1}{\partial \xi_2}\frac{\partial U_0}{\partial \xi_1} + \frac{1}{a_1 a_2^2}\frac{\partial a_2}{\partial \xi_1}\frac{\partial U_0}{\partial \xi_2}\\
&\left.+\frac{1}{a_2}\frac{\partial U_0}{\partial \xi_1}\frac{\partial}{\partial \xi_2}\left(\frac{1}{a_1}\right) - \frac{1}{a_1}\frac{\partial U_0}{\partial \xi_2}\frac{\partial}{\partial \xi_1}\left(\frac{1}{a_2}\right) + \frac{1}{a_2}\frac{\partial V_0}{\partial \xi_2}\frac{\partial}{\partial \xi_2}\left(\frac{1}{a_2}\right)\right\},
\end{aligned} \tag{3.23}$$

and

$$\rho_a \left\{ \frac{\partial W_0}{\partial t} + \frac{\partial \xi_1}{\partial t}\frac{\partial W_0}{\partial \xi_1} + \frac{\partial \xi_2}{\partial t}\frac{\partial W_0}{\partial \xi_2} + \frac{U_0}{a_1}\frac{\partial W_0}{\partial \xi_1} + \frac{V_0}{a_2}\frac{\partial W_0}{\partial \xi_2} \right\}$$

$$+M_0\frac{\partial W_1}{\partial \eta} + \kappa_1 U_0^2 + \kappa_2 V_0^2 = -\frac{\partial P_1}{\partial \eta}$$

$$+\frac{Pr}{3}\left\{ \frac{\kappa}{a_1 a_2}\left(\frac{\partial}{\partial \xi_1}(a_2 U_0) + \frac{\partial}{\partial \xi_2}(a_1 V_0) \right) + \frac{1}{a_1 a_2}\frac{\partial}{\partial \eta}\left(\frac{\partial}{\partial \xi_1}(a_2 U_1) + \frac{\partial}{\partial \xi_2}(a_1 V_1) \right) \right.$$

$$\left. -\frac{1}{a_1 a_2}\frac{\partial}{\partial \xi_1}(a_2 \kappa_2 U_0) - \frac{1}{a_1 a_2}\frac{\partial}{\partial \xi_2}(a_1 \kappa_1 V_0) + (2\kappa_1\kappa_2 - \kappa^2)W_0 - \kappa\frac{\partial W_1}{\partial \eta} + \frac{\partial^2 W_2}{\partial \eta^2} \right\}$$

$$+Pr\left\{ \frac{1}{a_1 a_2}\frac{\partial}{\partial \xi_1}\left(\frac{a_2}{a_1}\frac{\partial W_0}{\partial \xi_1} \right) + \frac{1}{a_1 a_2}\frac{\partial}{\partial \xi_2}\left(\frac{a_1}{a_2}\frac{\partial W_0}{\partial \xi_2} \right) + (2\kappa_1\kappa_2 - \kappa^2)W_0 \right.$$

$$-\kappa\frac{\partial W_1}{\partial \eta} + \frac{\partial^2 W_2}{\partial \eta^2} + \frac{U_0\kappa_1}{a_1 a_2}\frac{\partial a_2}{\partial \xi_1} + \frac{V_0\kappa_2}{a_1 a_2}\frac{\partial a_1}{\partial \xi_2} + \frac{U_0}{a_1}\frac{\partial \kappa_1}{\partial \xi_1} + \frac{V_0}{a_2}\frac{\partial \kappa_2}{\partial \xi_2} - \frac{U_0}{a_1 a_2}\frac{\partial (a_2\kappa_2)}{\partial \xi_1}$$

$$\left. + \frac{\kappa}{a_1 a_2}\left(U_0\frac{\partial a_2}{\partial \xi_1} + V_0\frac{\partial a_1}{\partial \xi_2} \right) - \frac{V_0}{a_1 a_2}\frac{\partial}{\partial \xi_2}(a_1\kappa_1) + 2\frac{\kappa_1}{a_1}\frac{\partial U_0}{\partial \xi_1} + 2\frac{\kappa_2}{a_2}\frac{\partial V_0}{\partial \xi_2} \right\}. \tag{3.24}$$

When the first equation, (3.22), is integrated across the reaction zone and use is made of (3.20) and its differentiated form

$$\int_{-\infty}^{\infty} \frac{\partial P_0}{\partial \xi_1}\,\mathrm{d}\eta = \lim_{\eta\to\infty}\left(\eta\frac{\partial p_0^+}{\partial \xi_1} \right) - \lim_{\eta\to-\infty}\left(\eta\frac{\partial p_0^-}{\partial \xi_1} \right) + \tfrac{4}{3}Pr\left[\frac{\partial w_1}{\partial \xi_1} \right],$$

one finds the following jump relationship:

$$\left[\frac{\partial u_1}{\partial n} \right] = \frac{1}{a_1}\left[\frac{\partial w_1}{\partial \xi_1} \right]. \tag{3.25}$$

In a similar way, the other two equations yield

$$\left[\frac{\partial v_1}{\partial n} \right] = \frac{1}{a_2}\left[\frac{\partial w_1}{\partial \xi_2} \right], \tag{3.26}$$

$$[p_1] + m_0[w_1] = \tfrac{4}{3}Pr\left\{ \left[\frac{\partial w_1}{\partial n} \right] - \kappa[w_1] \right\} + \tfrac{1}{3}Pr\frac{1}{a_1 a_2}\left[\frac{\partial (a_2 u_1)}{\partial \xi_1} + \frac{\partial (a_1 v_1)}{\partial \xi_2} \right]. \tag{3.27}$$

3.3. *Energy and species*

As before, we introduce the stretching transformation and the inner expansions (3.8) in the energy and species equations (2.12)–(2.14), written in terms of the intrinsic coordinates, to obtain equations for the τ_i, y_i and x_i. When the energy and species equations are added, so as to eliminate the nonlinear reaction term, one finds to $O(\theta^{-1})$ and $O(\theta^{-2})$ the linear equations

$$\frac{\partial^2}{\partial \eta^2}\left(\tau_1 + \frac{1}{L_F}y_1 \right) = 0, \qquad \frac{\partial^2}{\partial \eta^2}\left(\tau_1 + \frac{1}{L_X}x_1 \right) = 0, \tag{3.28}$$

$$\frac{\partial^2}{\partial\eta^2}\left(\tau_2+\frac{1}{L_F}y_2\right)=M_0\frac{\partial}{\partial\eta}(\tau_1+y_1)+\kappa\frac{\partial}{\partial\eta}\left(\tau_1+\frac{1}{L_F}y_1\right), \tag{3.29}$$

$$\frac{\partial^2}{\partial\eta^2}\left(\tau_2+\frac{1}{L_X}x_2\right)=M_0\frac{\partial}{\partial\eta}(\tau_1+x_1)+\kappa\frac{\partial}{\partial\eta}\left(\tau_1+\frac{1}{L_X}x_1\right), \tag{3.30}$$

which provide relations between the mass fractions and the temperature perturbations. These equations are to be integrated subject to the matching conditions

$$\left.\begin{aligned}
&\tau_1\sim\frac{\partial T_0}{\partial n}\bigg|^{\pm}\eta+T_1^{\pm}, \quad \tau_2\sim\frac{1}{2}\frac{\partial^2 T_0}{\partial n^2}\bigg|^{\pm}\eta^2+\frac{\partial T_1}{\partial n}\bigg|^{\pm}\eta+T_2^{\pm},\\
&y_1\sim\frac{\partial Y_0}{\partial n}\bigg|^{\pm}\eta+Y_1^{\pm}, \quad y_2\sim\frac{1}{2}\frac{\partial^2 Y_0}{\partial n^2}\bigg|^{\pm}\eta^2+\frac{\partial Y_1}{\partial n}\bigg|^{\pm}\eta+Y_2^{\pm},\\
&x_1\sim\frac{\partial X_0}{\partial n}\bigg|^{\pm}\eta+X_1^{\pm}, \quad x_2\sim\frac{1}{2}\frac{\partial^2 X_0}{\partial n^2}\bigg|^{\pm}\eta^2+\frac{\partial X_1}{\partial n}\bigg|^{\pm}\eta+X_2^{\pm},
\end{aligned}\right\} \tag{3.31}$$

as $\eta\to\pm\infty$. Integrating (3.28) once yields the jump relationships

$$\left[\frac{\partial T_0}{\partial n}\right]=-\frac{1}{L_F}\left[\frac{\partial Y_0}{\partial n}\right]=-\frac{1}{L_X}\left[\frac{\partial X_0}{\partial n}\right], \tag{3.32}$$

which reflect that, to leading order, the fuel and oxidant flow into the reaction sheet in stoichiometric proportion. A second integration provides the expressions

$$\tau_1+\frac{1}{L_F}y_1=\frac{\partial T_0}{\partial n}\bigg|^{+}\eta+T_1^{+}+\frac{1}{L_F}Y_1^{+}, \tag{3.33}$$

$$\tau_1+\frac{1}{L_X}x_1=\frac{\partial T_0}{\partial n}\bigg|^{-}\eta+T_1^{-}+\frac{1}{L_X}X_1^{-}, \tag{3.34}$$

as well as the jump conditions

$$[T_1]=-\frac{1}{L_F}[Y_1]=-\frac{1}{L_X}[X_1]. \tag{3.35}$$

Now, integrating (3.29)–(3.30) once across the reaction zone yields the jump conditions

$$\left[m_0T_1-\frac{\partial T_1}{\partial n}\right]=-\left[m_0Y_1-\frac{1}{L_F}\frac{\partial Y_1}{\partial n}\right]=-\left[m_0X_1-\frac{1}{L_X}\frac{\partial X_1}{\partial n}\right]; \tag{3.36}$$

the information resulting from a second integration will not be needed in the present discussion.

We now turn our attention to the energy equation

$$\frac{\partial^2\tau_1}{\partial\eta^2}=-D\,x_1y_1\mathrm{e}^{\tau_1} \tag{3.37}$$

which, after substituting (3.33) and (3.34) for y_1 and x_1, yields a nonlinear equation for the temperature perturbation τ_1, uncoupled from all other variables. By introducing the transformation

$$\tau_1=-\delta^{-1/3}(\varphi+\gamma\zeta)+\frac{1+\gamma}{2}h_X^*+\frac{1-\gamma}{2}h_F^*,$$

$$\eta=-\{2\delta^{-1/3}\zeta+h_F^*-h_X^*\}\left[\frac{\partial T_0}{\partial n}\right]^{-1},$$

this equation, together with the corresponding matching conditions, can be reduced to a simpler form which involves only two parameters:

$$\gamma = -\frac{\left.\dfrac{\partial T_0}{\partial n}\right|^{-} + \left.\dfrac{\partial T_0}{\partial n}\right|^{+}}{\left.\dfrac{\partial T_0}{\partial n}\right|^{-} - \left.\dfrac{\partial T_0}{\partial n}\right|^{+}} \tag{3.38}$$

and

$$\delta = 4L_F L_X D \left[\frac{\partial T_0}{\partial n}\right]^{-2} \exp\left\{\frac{1+\gamma}{2}h_X^* + \frac{1-\gamma}{2}h_F^*\right\}. \tag{3.39}$$

Here h_F^* and h_X^* are the excess/deficiency in the fuel and oxidant enthalpies, respectively, given by

$$h_F^* = T_1^+ + \frac{1}{L_F}Y_1^+, \qquad h_X^* = T_1^- + \frac{1}{L_X}X_1^-.$$

The equation, and the corresponding matching conditions that follow from (3.31), now become

$$\frac{\partial^2 \varphi}{\partial \zeta^2} = (\varphi^2 - \zeta^2)\exp\left[-\delta^{-1/3}(\varphi + \gamma\zeta)\right], \tag{3.40}$$

$$\frac{\partial \varphi}{\partial \zeta} \sim -1 \quad \text{as } \zeta \to -\infty, \qquad \frac{\partial \varphi}{\partial \zeta} \sim 1 \quad \text{as } \zeta \to +\infty, \tag{3.41}$$

and

$$X_1^- = L_X S_X, \qquad S_X = \delta^{-1/3}\lim_{\zeta \to -\infty}(\varphi + \zeta), \tag{3.42}$$

$$Y_1^+ = L_F S_F, \qquad S_F = \delta^{-1/3}\lim_{\zeta \to +\infty}(\varphi - \zeta). \tag{3.43}$$

The boundary value problem (3.40)–(3.41) which determines $\varphi(\zeta;\gamma,\delta)$ is identical to that previously written by Linan (1974) in analysing the counterflow diffusion flame. As noted later, the general formulation based on a mixture fraction coordinate (Peters 1983, 1986) also results in this same problem. In both cases, however, unity Lewis numbers were assumed. The generalization here applies to a general two-dimensional reaction sheet and is not restricted to unity Lewis numbers. Once the solution φ is known, the quantities S_F and S_X can be calculated and these, in turn, determine Y_1^+ and X_1^-. Note that the conditions (3.42) and (3.43) signify that fuel and oxidant are not necessarily completely consumed in the reaction zone. There are, in general, $O(\theta^{-1})$ amounts of fuel and oxidant that pass through the reaction zone unburned. As we shall see, the quantities S_F and S_X, which are proportional to the reactants leakage Y_1^+ and X_1^- respectively, are needed to complete the formulation of the problem to $O(\theta^{-1})$.

The reduced problem for φ depends only on the two parameters γ and δ. The parameter γ is the ratio of the excess heat conducted to one side of the reaction sheet to the total heat generated in the reaction zone. When $\gamma = 0$ there are equal fluxes of heat directed away from the reaction sheet; the symmetry of the problem then implies that $S_F = S_X$. If $\gamma > 0$ more heat is transported to the oxidant side; if $\gamma < 0$ more heat is transported to the fuel side. Typically, the temperature peaks at the reaction sheet which implies that $[\partial T_0/\partial n] < 0$ and, unless the supply temperatures exceed

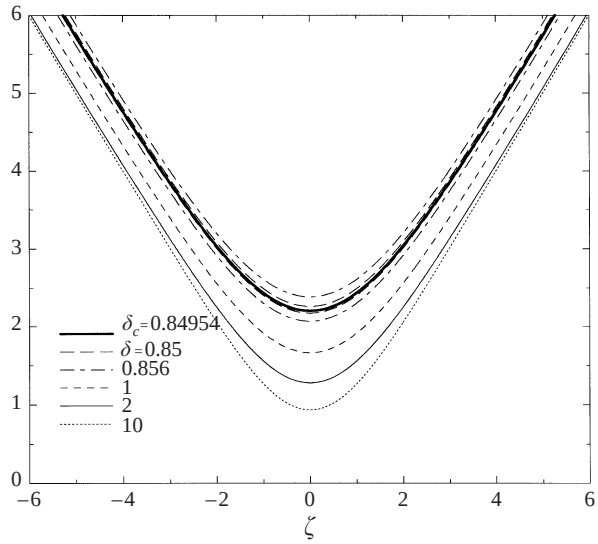

FIGURE 2. Solutions of the inner structure equation for $\gamma = 0$. Note that for $\delta > \delta_c = 0.84954$ there are two distinct solutions, symmetric with respect to ζ.

the adiabatic temperature T_a, a case that we do not consider here, $-1 < \gamma < 1$.† The parameter δ measures the intensity of the chemical reaction rate. As $\delta \to \infty$, a limit reached when the Damköhler number D is infinitely large, the exponential in equation (3.40) tends to 1 and the problem reduces to

$$\frac{\partial^2 \varphi}{\partial \zeta^2} = \varphi^2 - \zeta^2, \qquad \frac{\partial \varphi}{\partial \zeta} \sim \pm 1 \quad \text{as } \zeta \to \pm\infty,$$

which possesses a unique solution (found numerically) such that $\varphi \sim \pm\zeta + o(1)$ as $\zeta \to \pm\infty$. Then $S_F = S_X = 0$. This limit corresponds to the Burke–Schumann limit of complete combustion.

It should be noted that, due to the symmetry of the boundary value problem (3.40)–(3.41) with respect to $\gamma\zeta$, it suffices to consider $0 \leqslant \gamma < 1$ only. It is easily seen that $\varphi(\zeta; -\gamma, \delta) = \varphi(-\zeta; \gamma, \delta)$ so that, when γ is negative, S_F is simply obtained from S_X by replacing γ with $-\gamma$. In attempting to define the functions $S_F(\gamma, \delta)$ and $S_X(\gamma, \delta)$ we shall be concerned with $\gamma > 0$ with the understanding that $S_F(-\gamma, \delta) = S_X(\gamma, \delta)$ and $S_X(-\gamma, \delta) = S_F(\gamma, \delta)$.

Numerical solutions of the boundary value problem (3.40)–(3.41) were obtained using COLSYS, an ODE integrator that uses a collocation method (see Asher, Christiansen & Russel 1981). Representative solutions for several values of δ are shown in figures 2 and 3 for two values of γ. Figure 2 corresponds to $\gamma = 0$ and, as expected, the solutions are symmetric with respect to $\zeta = 0$. Note that for $\delta = 0.856$ there are two curves, one on each side of the curve corresponding to $\delta = \delta_c = 0.84954$ (the dark curve in the figure). Similarly, there are two distinct solutions for all $\delta > \delta_c$. Figure 3, which corresponds to $\gamma = 0.4$, shows a similar behaviour except that now the solutions are no longer symmetric with respect to $\zeta = 0$. Thus, for δ larger than a critical value δ_c, the solution is multi-valued, there is a unique solution for $\delta = \delta_c$ and

† When $|\gamma| > 1$ there is a net heat flux directed towards the reaction sheet and, correspondingly an $O(1)$ rather than $O(1/\theta)$ leakage of fuel and/or oxidant. A different asymptotic treatment is required in this case.

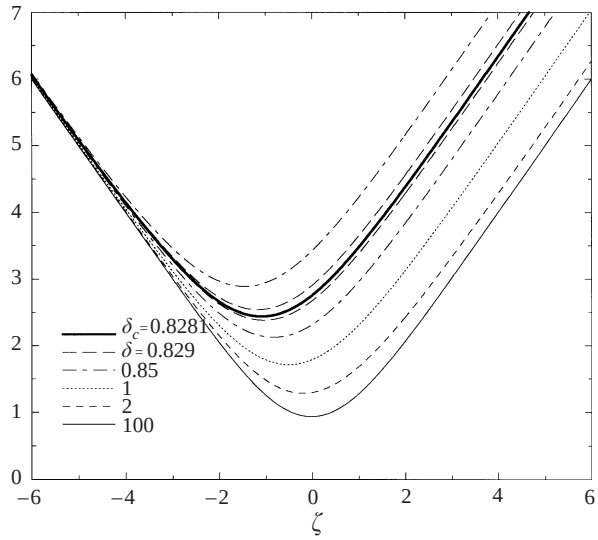

FIGURE 3. Solutions of the inner structure equation for $\gamma = 0.4$. Note that for $\delta > \delta_c = 0.8281$ there are two distinct solutions which are no longer symmetric with respect to ζ.

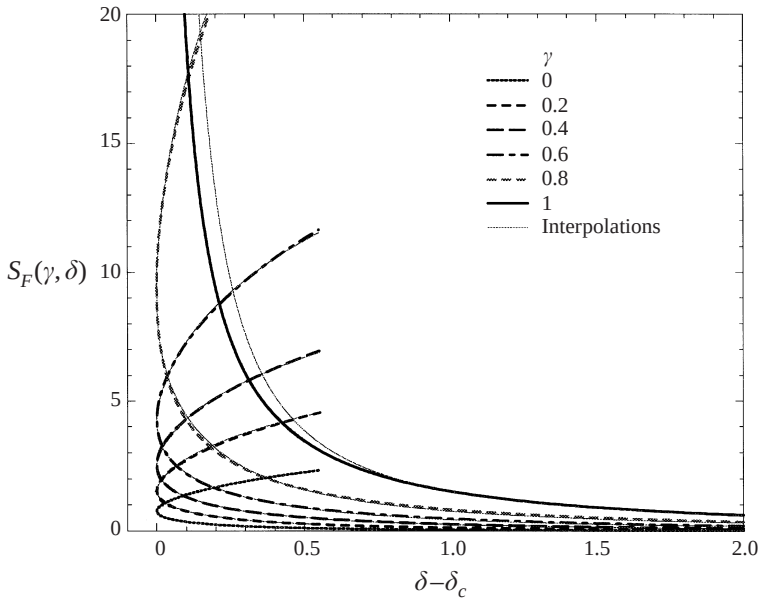

FIGURE 4. Interpolated and exact numerical values of S_F versus $\delta - \delta_c$.

no solution for $\delta < \delta_c$. The critical value δ_c depends solely on γ. Based on numerical computations, Linan (1974) provides an approximation for δ_c as

$$\delta_c = \exp(1)\{(1-|\gamma|) - (1-|\gamma|)^2 + 0.26(1-|\gamma|)^3 + 0.055(1-|\gamma|)^4\}. \tag{3.44}$$

Hence, for moderate values of $\delta > \delta_c$ the system has two physically relevant solutions; two different quantities of the reactants leakage S_F and S_X are possible. This is illustrated in figures 4 and 5, which show the dependence of S_F and S_X on $\delta - \delta_c$ for

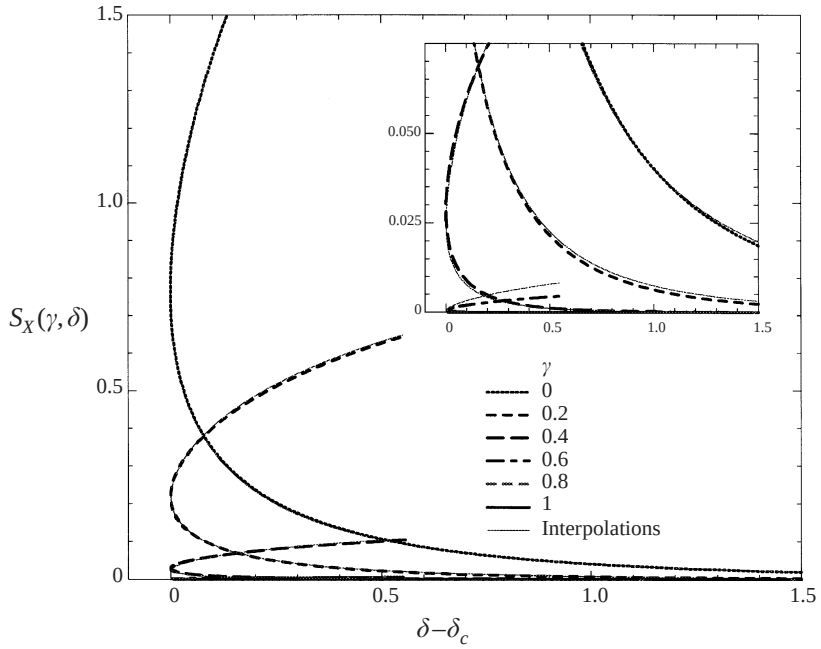

FIGURE 5. Interpolated and exact numerical values of S_X versus $\delta - \delta_c$.

various values of γ. For a given δ the solution on the lower branch, in contrast to its counterpart on the upper branch, corresponds to a state with a higher temperature and smaller fuel and oxidant leakages. The solutions on the lower branch tend to the Burke–Schumann limit of complete combustion when $\delta \to \infty$. The solutions on the upper branch correspond to states with increasingly large reactant leakage and thus become invalid when δ is sufficiently large. We also note from the figures that when $\gamma = 0$ the temperature profile in the reaction zone is symmetric: there is an equal flux of heat directed towards the fuel as towards the oxidant and $S_F = S_X$. When $\gamma > 0$, more heat is conducted towards the oxidant side ($\zeta \to -\infty$) which, consequently, is more completely consumed, namely $S_X < S_F$. The reverse is true when $\gamma < 0$. At $\delta = \delta_c$ we see that $S_F \to \infty$ and $S_X \to 0$ as $\gamma \to 1$; and similarly $S_X \to \infty$ and $S_F \to 0$ as $\gamma \to -1$.

From the expression (3.39) for δ it is clear that solutions likewise exist only for values of the Damköhler number D above a critical value, D_{ex}. No burning is possible for $D < D_{\text{ex}}$ and, since D is a physically controllable parameter, D_{ex} identifies the extinction condition. We note that when the available enthalpies associated with the fuel and oxidant h_F^* and h_X^* both vanish, the parameter δ is proportional to the Damköhler number D. Consequently $\delta_c \propto D_{\text{ex}}$ and they both represent the same physical state – the critical state below which burning is no longer possible. Generally speaking, this will be the case when the Lewis numbers are both equal to 1; the enthalpies $T + Y$ and $T + X$ are now conserved scalars (i.e. each satisfy an equation with no chemical-source term) and the exact solution can be written for these quantities without recourse to the large-activation-energy approximation. Any perturbation must therefore be equal to zero so that $h_F^* = h_X^* = 0$. When the available enthalpies are not zero, the expression (3.39) is an implicit relation for the determination of δ because h_F^* and h_X^* depend on the reactants leakage S_F and S_X which, in turn, depend on δ. As a result, δ_c does not necessarily correspond to D_{ex} and

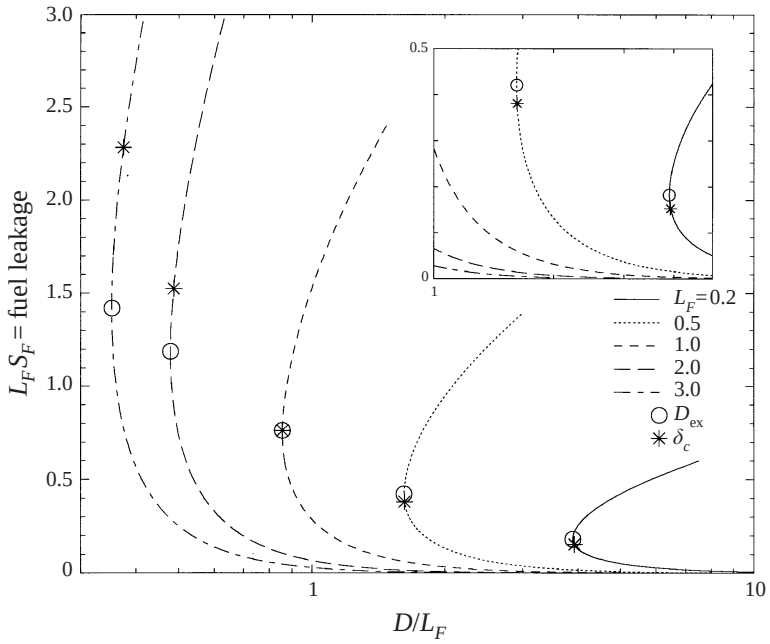

FIGURE 6. Response curves of $S_F \sim$ fuel leakage versus the Damköhler number D for several values of L_F; calculated for $L_X = 1.0$, $\phi = 1$, $\gamma = 0$. The star marks the state corresponding to δ_c; the circle marks the state corresponding to extinction.

so does not identify the extinction condition. This has been previously recognized by Kim & Williams (1997). To clarify this point further we have marked on the response curve in figure 6 the state corresponding to δ_c. The graph shows the dependence of the fuel leakage $L_F S_F$ on the Damköhler number D/L_F. We note that the state corresponding to δ_c coincides with D_{ex} when $L_F = 1$; it corresponds to a state on the lower branch of the response curve for $L_F < 1$ and to a state on the upper branch of the response curve when $L_F > 1$. Although the results in this figure are illustrated for the case $\gamma = 0$, $L_X = 1$, the demonstrated trend appears to be quite general.

We note that unity Lewis numbers is not a sufficient condition for the exponent in (3.39) to vanish. Although in this case the enthalpies $T + Y$ and $T + X$ satisfy equations with no chemical-source term, the boundary conditions associated with these quantities could be coupled to the remaining equations in such a way as to give rise to non-zero h_F^* and h_X^*. This was found to be the case when analysing the structure of burner-generated spherical diffusion flames (Mills & Matalon 1997, 1998); the drop in the available enthalpies in that case was associated with heat losses, either to the surface of the burner or by thermal radiation. In the latter δ_c was associated with two values of D, lower and upper limits beyond which no burning is possible.

The curves shown in figures 4 and 5 were generated numerically. The graphs were subsequently used to write down interpolations for S_F and S_X as functions of δ and γ. This was done with the help of KaleidaGraph (Abelbeck Software, copyright 1994, version 3.04). The interpolations are presented here only for $0 \leqslant \gamma < 1$ because, and as noted earlier, S_F and S_X must be interchanged when $-1 < \gamma \leqslant 0$. Separate

interpolations were found for the upper branches and lower branches of these curves, as follows.

Lower branch

$$S_F = a_0\,\delta^{-4/3}\exp\{-a_1(\delta-\delta_c)^{a_2}\}, \tag{3.45}$$

$$a_0 = 0.61923 + 3.2523\gamma + 0.52069\,\gamma^2,$$

$$a_1 = 1.9077 - 1.901\gamma + 1.055\,\gamma^2,$$

$$a_2 = 0.46137 - 0.15374\,\gamma - 0.06769\,\gamma^4 - 0.23288\,\gamma^6;$$

$$S_X = b_0\delta^{-4/3}\exp\{-b_1(\delta-\delta_c)^{b_2}\}, \tag{3.46}$$

$$b_0 = 0.61923\,(1-\gamma)^{15}\exp\{10.469\,\gamma\},$$

$$b_1 = 1.9077 + 11.588\,\gamma^2 - 17.014\,\gamma^4 + 55.865\,\gamma^6,$$

$$b_2 = 0.46137 + 0.27706\,\gamma - 0.2029\,\gamma^2.$$

These expressions reflect the following properties of the exact numerical solution: $S_F \to 0$ and $S_X \to 0$ as $\delta \to \infty$; $S_F = S_X$ for $\gamma = 0$; $\partial S_F/\partial\delta \to -\infty$ and $\partial S_X/\partial\delta \to -\infty$ as $\delta \to \delta_c$; $S_X \equiv 0$ for $\gamma = 1$.

Upper branch

$$S_F = \delta^{-1/3}\{q_0 + q_1(\delta-\delta_c)^{q_2}\}, \tag{3.47}$$

$$q_0 = 0.72704\,(1-\gamma)^{-0.63858}\exp(1.4311\gamma^{0.5696}),$$

$$q_1 = 2.7108 + \frac{10.788\tan(\pi\gamma/2)}{1 + 2.5459\gamma - 2.8114\gamma^2},$$

$$q_2 = 0.625;$$

$$S_X = \delta^{-1/3}\{r_0 + r_1(\delta-\delta_c)^{r_2}\}, \tag{3.48}$$

$$r_0 = 0.72704\,(1-\gamma)^{15}\exp(10.451\gamma),$$

$$r_1 = 2.7108\,(1-\gamma)^{5.8507},$$

$$r_2 = 0.625 - 0.49221\gamma + 2.0203\,\gamma^2 - 4.2464\,\gamma^3 + 4.2286\,\gamma^4.$$

These expressions reflect the following properties of the exact numerical solution: $S_F \to \infty$ and $S_X \to \infty$ as $\delta \to \infty$; $S_F = S_X$ for $\gamma = 0$; $\partial S_F/\partial\delta \to \infty$ and $\partial S_X/\partial\delta \to \infty$ as $\delta \to \delta_c$; $S_F \to \infty$ and $S_X \to 0$ as $\gamma \to 1$ for every δ. We also note that the fuel and oxidant leakage at extinction are given simply by $S_F = \delta^{-1/3}q_0$ and $S_X = \delta^{-1/3}r_0$, respectively. Finally, we point out that the numerical result and the interpolations are both plotted in figures 4 and 5. With the exception of the case $\gamma = 1$, where the asymptotic analysis becomes strictly invalid, the agreement is excellent.

3.4. *Mixture fraction formulation*

In this section we show that our formulation reduces to Peter's mixture fraction formulation (Peters 1983, 1986) when *unity Lewis numbers* is assumed. For a one-step

chemistry a convenient definition of the mixture fraction Z is

$$Z = \frac{Y - X + X_\infty}{1 + X_\infty},$$

where X_∞ is the oxidant mass fraction at the oxidant boundary. Note that, since we have used $\nu \tilde{Y}_{-\infty}$ as a unit for the oxidant mass fraction,

$$X_\infty = \frac{\tilde{X}_\infty / \nu_X W_X}{\tilde{Y}_{-\infty} / \nu_F W_F} = \frac{1}{\phi}$$

is the initial 'mixture strength', namely the ratio of oxidant mass fraction supplied to the oxidant side to the fuel mass fraction supplied to the fuel side normalized by the stoichiometric proportions. Its reciprocal, ϕ, can be considered as an 'equivalence ratio' based on the supply conditions. The mixture fraction thus defined varies between zero and 1; it is zero at the oxidant boundary and 1 in the fuel stream. Furthermore, it satisfies

$$\rho \frac{\mathrm{D}Z}{\mathrm{D}t} - \nabla^2 Z = (1 - L_X^{-1})\nabla^2 X - (1 - L_F^{-1})\nabla^2 Y \tag{3.49}$$

so that, when $L_F = L_X = 1$, the right-hand side vanishes and the mixture fraction Z is a conserved scalar (provided of course that the boundary conditions do not introduce additional source terms).

The stoichiometric value of the mixture fraction is given by $Z_{\mathrm{st}} = X_\infty/(1 + X_\infty) = (1+\phi)^{-1}$ so that $Z(\boldsymbol{x}, t) - Z_{\mathrm{st}} = 0$ represents the stoichiometric level surface. For unity Lewis numbers this representation is identical to $F(\boldsymbol{x}, t) = 0$ so that $\boldsymbol{n} = -\nabla Z/|\nabla Z|$. A coordinate transformation from $\{x, y, z, t\}$ to $\{x, y, Z(x, y, z), t\}$ readily implies that

$$-\frac{\partial}{\partial n} = |\nabla Z| \frac{\partial}{\partial Z} + \frac{\nabla Z \cdot \nabla_{\mathrm{T}}}{|\nabla Z|}, \qquad \nabla_{\mathrm{T}} \equiv (\partial_x, \partial_y)$$

so that

$$\left[\frac{\partial T}{\partial n}\right]^2 = |\nabla Z|^2 \left[\frac{\partial T}{\partial Z}\right]^2.$$

Since T also satisfies reaction-free equations on either side of the reaction sheet, it may be expressed as a linear combination of Z, namely

$$T = \begin{cases} T_\infty + (1 + T_{-\infty} - T_\infty)Z, & 0 < Z < Z_{\mathrm{st}} \\ T_{-\infty} + (X_\infty - T_{-\infty} - T_\infty)(1 - Z), & Z_{\mathrm{st}} < Z < 1, \end{cases}$$

where $T_{-\infty}$ and T_∞ denote the temperatures far away in the fuel and oxidant regions, respectively. The common value at $Z = Z_{\mathrm{st}}$ is the adiabatic flame temperature T_a given by

$$T_a = T_\infty + (1 + T_{-\infty} - T_\infty)(1 + \phi)^{-1}. \tag{3.50}$$

Also one finds that $[\partial T/\partial Z]^2 = (1 - Z_{\mathrm{st}})^{-2}$ so that

$$\delta = \frac{4(1 - Z_{\mathrm{st}})^2}{|\nabla Z|^2} D$$

is inversely proportional to the scalar dissipation rate $\chi \equiv |\nabla Z|^2$ (which in dimensional form is defined as $\tilde{\chi} = \mathscr{D}|\nabla Z|^2$ and has therefore units of $1/\mathrm{s}$). We also note that the description of the reaction zone requires introducing the stretching transformation $\xi = (Z - Z_{\mathrm{st}})/\theta$; one then recovers the structure equation (3.37) but with the left-hand side replaced by $|\nabla Z|^2(\partial^2 \tau_1/\partial \xi^2)$ as in Peters (1983); see also Linan & Williams (1993).

As a final comment we would like to mention that for non-unity Lewis numbers the stoichiometric level surface $F = 0$, which we have identified as the reaction sheet to within $O(\theta^{-1})$, does not coincide with the surface $Z = Z_{\rm st}$. In this case Z is no longer a conserved scalar, as is clear from (3.49), and the jump conditions across $Z = Z_{\rm st}$ are not obvious. As a result of preferential diffusion, iso-contours of Z would be denser in some regions than in others so that profiles of temperature and concentration would no longer depend solely on Z. Attempts to generalize the definition of the mixture fraction, by weighting the mass fractions with the corresponding Lewis number, lead to cumbersome expressions that do not resolve this difficulty.

4. Summary–the model

The derivation in the previous section shows that, for a large activation energy, the problem simplifies to a free boundary problem: the chemical activity is confined to a sheet, $F(\boldsymbol{x}, t) = 0$, on either side of which one only needs to solve the reaction-free equations, i.e. equations (2.10)–(2.15) with $\omega = 0$. The jump conditions across the reaction sheet, carried out to $O(\theta^{-1})$, adjust the variables so as to account for the heat release and the degree of fuel and oxidant consumption that take place in the reaction zone. Here we summarize the results and express them in a coordinate-free form.

To leading order, the following jump relationships must be satisfied across $F = 0$:

$$[T_0] = [Y_0] = [X_0] = 0, \tag{4.1}$$

$$\left[\frac{\partial T_0}{\partial n}\right] = -\frac{1}{L_F}\left[\frac{\partial Y_0}{\partial n}\right] = -\frac{1}{L_X}\left[\frac{\partial X_0}{\partial n}\right], \tag{4.2}$$

$$[\boldsymbol{v}_0 \cdot \boldsymbol{n}] = 0, \qquad [\boldsymbol{n} \times (\boldsymbol{v}_0 \times \boldsymbol{n})] = 0, \tag{4.3}$$

$$\left[\frac{\partial}{\partial n}(\boldsymbol{v}_0 \cdot \boldsymbol{n})\right] = m_0\left[\frac{\partial T_0}{\partial n}\right], \qquad \left[\frac{\partial}{\partial n}(\boldsymbol{n} \times (\boldsymbol{v}_0 \times \boldsymbol{n}))\right] = 0, \tag{4.4}$$

$$[p_0] = \tfrac{4}{3} Pr\left[\frac{\partial}{\partial n}(\boldsymbol{v}_0 \cdot \boldsymbol{n})\right]. \tag{4.5}$$

These, together with the requirements of complete combustion, namely

$$Y_0\big|_{F=0} = X_0\big|_{F=0} = 0, \tag{4.6}$$

suffice to solve the equations and determine the unknown function $F(\boldsymbol{x}, t)$. The unit normal $\boldsymbol{n}$, and the velocity of the surface V_f are given by

$$\boldsymbol{n} = \frac{\nabla F}{|\nabla F|}, \qquad V_f = -\frac{1}{|\nabla F|}\frac{\partial F}{\partial t},$$

respectively. Note that the velocity vector was decomposed into its normal and tangential components, $\boldsymbol{v} = \boldsymbol{v} \cdot \boldsymbol{n} + \boldsymbol{n} \times (\boldsymbol{v} \times \boldsymbol{n})$, and that $m = \rho(\boldsymbol{v} \cdot \boldsymbol{n} - V_f)|_{F=0}$ is the mass flux normal to the reaction sheet. Finally, we point out that once the solution is determined, the parameter γ can be evaluated at every point along the sheet.

To $O(\theta^{-1})$, the following jump relationships must be satisfied across $F = 0$:

$$[T_1] = -\frac{1}{L_F}[Y_1] = -\frac{1}{L_X}[X_1], \tag{4.7}$$

$$\left[m_0 T_1 - \frac{\partial T_1}{\partial n}\right] = -\left[m_0 Y_1 - L_F^{-1}\frac{\partial Y_1}{\partial n}\right] = -\left[m_0 X_1 - L_X^{-1}\frac{\partial X_1}{\partial n}\right], \tag{4.8}$$

$$[\boldsymbol{v}_1 \cdot \boldsymbol{n}] = m_0[T_1], \qquad [\boldsymbol{n} \times (\boldsymbol{v}_1 \times \boldsymbol{n})] = 0, \tag{4.9}$$

$$\left[\frac{\partial}{\partial n}(\rho_0 \boldsymbol{v}_1 + \rho_1 \boldsymbol{v}_0)\cdot \boldsymbol{n}\right] = -\left[\frac{\partial \rho_1}{\partial t}\right] + \kappa[(\rho_0 \boldsymbol{v}_1 + \rho_1 \boldsymbol{v}_0)\cdot \boldsymbol{n}] - [\nabla \cdot (\boldsymbol{n} \times ((\rho_0 \boldsymbol{v}_1 + \rho_1 \boldsymbol{v}_0) \times \boldsymbol{n}))], \tag{4.10}$$

$$\left[\frac{\partial}{\partial n}(\boldsymbol{n} \times (\boldsymbol{v}_1 \times \boldsymbol{n}))\right] = [\nabla_\perp (\boldsymbol{v}_1 \cdot \boldsymbol{n})], \tag{4.11}$$

$$[p_1] = -m_0^2[T_1] + \tfrac{4}{3}Pr\left\{\left[\frac{\partial}{\partial n}(\boldsymbol{v}_1 \cdot \boldsymbol{n})\right] - \kappa[\boldsymbol{v}_1 \cdot \boldsymbol{n}]\right\} + \tfrac{1}{3}Pr\,[\nabla \cdot (\boldsymbol{n} \times (\boldsymbol{v}_1 \times \boldsymbol{n}))], \tag{4.12}$$

where $\nabla_\perp$ denotes the surface gradient, namely $\nabla \equiv \nabla_\perp + \boldsymbol{n}\,\partial/\partial n$. These together with the conditions

$$Y_1\big|_{F=0^+} = L_F\, S_F(\gamma, \delta), \qquad X_1\big|_{F=0^-} = L_X\, S_X(\gamma, \delta), \tag{4.13}$$

where δ is given implicitly by

$$\delta = 4L_F L_X D \left[\frac{\partial T_0}{\partial n}\right]^{-2} \exp\left\{\frac{1+\gamma}{2}h_X^* + \frac{1-\gamma}{2}h_F^*\right\},$$

solve the equations at this order. Finally, we note that the relations (3.45)–(3.48) can be used for S_F and S_X without recourse to the numerical integration and that $h_F^* = T_1 + L_F^{-1}Y_1\big|_{F=0^+}$ and $h_X^* = T_1 + L_X^{-1}X_1\big|_{F=0^-}$ can be expressed in terms of S_F and S_X.

The location of the reaction sheet to $O(1)$ is defined quite naturally as the stoichiometric level surface, i.e. the location where the fuel and oxidant are completely consumed and the temperature reaches the adiabatic flame temperature. There is no such compelling criterion to identify an $O(\theta^{-1})$ correction to the location of the reaction sheet. Its determination is in fact arbitrary: any well-defined position within the infinitely wide reaction zone ($-\infty < \eta < \infty$) can be used for this purpose. One choice is clearly $\eta_f = 0$: the reaction sheet remains identified as the stoichiometric level surface up to $O(\theta^{-1})$. Any other choice introduces the additional unknown η_f into the formulation which consequently requires an appropriate condition for its determination. A natural choice is of course to identify η_f with the position η where the temperature τ_1 reaches its maximum value. This, however, is not a very convenient choice because τ_1 is only known numerically. Another possible choice is to identify η_f as the position where the temperature perturbation remains continuous to $O(\theta^{-1})$, namely to impose the condition

$$[T_1] + \eta_f \left[\frac{\partial T_0}{\partial n}\right] = 0. \tag{4.14}$$

This choice turns out to be convenient if one combines the expressions for the first two orders of the expansions in $1/\theta$. Thus, if the symbols identify the first two terms in the expansions (3.2), for example $T = T_0(\boldsymbol{x}, t) + \theta^{-1}T_1(\boldsymbol{x}, t)$ etc., we find that the jump conditions across $F(\boldsymbol{x}, t)$, which is now a distance η_f/θ from the stoichiometric

level surface, are as follows:

$$[T] = [Y] = [X] = 0,$$

$$\left[\frac{\partial T}{\partial n}\right] = -\frac{1}{L_F}\left[\frac{\partial Y}{\partial n}\right] = -\frac{1}{L_X}\left[\frac{\partial X}{\partial n}\right],$$

$$[\rho(\boldsymbol{v}\cdot\boldsymbol{n})] = 0, \qquad [\boldsymbol{n}\times(\boldsymbol{v}\times\boldsymbol{n})] = 0,$$

$$\left[\frac{\partial}{\partial n}\rho(\boldsymbol{v}\cdot\boldsymbol{n})\right] = -[\nabla\cdot(\boldsymbol{n}\times(\rho\boldsymbol{v}\times\boldsymbol{n})],$$

$$\left[\frac{\partial}{\partial n}(\boldsymbol{n}\times(\boldsymbol{v}\times\boldsymbol{n}))\right] = [\nabla_\perp(\boldsymbol{v}\cdot\boldsymbol{n})],$$

$$[p] = \tfrac{4}{3}Pr\left[\frac{\partial}{\partial n}(\boldsymbol{v}\cdot\boldsymbol{n})\right] + \tfrac{1}{3}Pr\,[\nabla\cdot(\boldsymbol{n}\times(\boldsymbol{v}\times\boldsymbol{n}))].$$

In addition, we have the requirements

$$Y\big|_{F=0^+} = L_F\,\theta^{-1}S_F(\gamma,\delta), \qquad X\big|_{F=0^-} = L_X\theta^{-1}S_X(\gamma,\delta),$$

with

$$\gamma = \left\{\frac{\partial T}{\partial n}\bigg|_{F=0^+} + \frac{\partial T}{\partial n}\bigg|_{F=0^-}\right\}\left[\frac{\partial T}{\partial n}\right]^{-1},$$

$$\delta = 4L_FL_XD\left[\frac{\partial T}{\partial n}\right]^{-2}\exp\left\{(T_f - T_a)\theta + \frac{1-\gamma}{2}S_F + \frac{1+\gamma}{2}S_X\right\},$$

where T_f is the flame temperature, i.e. the temperature at the reaction sheet, which differs from the adiabatic temperature T_a associated with complete combustion by an $O(\theta^{-1})$ amount.

5. Diffusive-thermal instability

In order to examine the onset of instability in diffusion flames and the dependence of the results on all relevant parameters, it is imperative to study a simple diffusion flame model not affected by external influences such as hydrodynamic or acoustic disturbances. It is well known that a steady, planar diffusion flame in a one-dimensional unbounded domain is not possible. While a planar diffusion flame can be established in the stagnation-point flow of two opposed jets, one of fuel and the other of oxidant, the flow field in this case is two-dimensional; the flame is under stretch, which generally exerts a strong stabilizing influence.† Thus, to retain one-dimensional simplicity, we consider the semi-infinite model as depicted in figure 7.

Fuel is fed from the bottom of a sufficiently long chamber at a constant velocity U. Conditions at the top of the chamber are maintained constant by a sufficiently fast flowing stream across the exit from which the oxidant diffuses inwards. Chemical reaction occurs within the chamber in a region centred near the location where fuel and oxidant meet at stoichiometric proportions. The combustion products that reach the top of the chamber are washed out by the cross-stream, thus ensuring that the conditions at the top remain as prescribed. It should be pointed out that the equivalent problem, in which oxidant is fed from the bottom of the chamber and fuel diffuses

† A modest stretch has a stabilizing influence. But when the stretch rate is large enough to threaten extinction, the instability can return, as shown in Buckmaster & Short (1999).

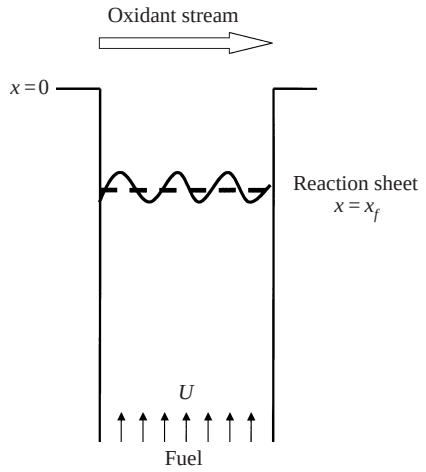

FIGURE 7. The one-dimensional flame configuration.

in from the top, can be readily discussed by interchanging the role played by the two reactants. However, as we shall see, the reactant introduced in the feed stream plays a special role in the stability properties. In the configuration shown in figure 7, for example, an observer sitting at the reaction zone sees a net mass flux directed from the fuel towards the oxidant side. In the reverse configuration, the 'inverse' diffusion flame, the net mass flux will be directed from the oxidant towards the fuel side.

Let the fuel concentration in the feed stream be $\tilde{Y}_{-\infty}$ and the oxidant concentration at the top of the chamber be $\tilde{X}_{\infty}$. The temperature far upstream, $\tilde{T}_{-\infty}$, and at the top of the chamber, $\tilde{T}_{\text{top}}$, are both scaled with respect to q/c_p, the characteristic temperature introduced earlier. In dimensionless form, the boundary conditions are therefore

$$T = T_{-\infty}, \quad Y = 1, \quad X = 0 \quad \text{as } x \to -\infty, \tag{5.1}$$

$$T = T_{-\infty} + \Delta T, \quad Y = 0, \quad X = \phi^{-1} \quad \text{at } x = 0, \tag{5.2}$$

where the temperature differential $\Delta T = c_p(\tilde{T}_{\text{top}} - \tilde{T}_{-\infty})/q$ can be positive or negative.

We invoke the constant-density approximation in order to suppress hydrodynamical disturbances, so that the flow field remains uniform and undisturbed. Hence $\rho = 1$ and $\boldsymbol{v} = 1\boldsymbol{i}$ and the (dimensionless) governing equations, to be solved on either side of the reaction sheet, simplify to

$$\frac{\partial T}{\partial t} + \frac{\partial T}{\partial x} - \nabla^2 T = 0, \tag{5.3}$$

$$\frac{\partial Y}{\partial t} + \frac{\partial Y}{\partial x} - \frac{1}{L_F}\nabla^2 Y = 0, \tag{5.4}$$

$$\frac{\partial X}{\partial t} + \frac{\partial X}{\partial x} - \frac{1}{L_X}\nabla^2 X = 0. \tag{5.5}$$

Across the reaction zone the only relevant jump relationships are (4.1), (4.2), (4.6) and (4.7), (4.8), (4.13).

5.1. *The steady planar flame*

The steady one-dimensional solution of this problem, describing a planar diffusion flame, expressed in power series of θ^{-1}as in (3.2) is

$$T \sim \begin{cases} T_{-\infty} + (\mathrm{e}^{-x_f} + \Delta T - 1)\mathrm{e}^{x} \\ \quad + \dfrac{T_a^2}{\theta}\left\{\dfrac{L_F}{L_X}\dfrac{(1-\mathrm{e}^{L_X x_f}) - L_X(1-\mathrm{e}^{x_f})}{1-\mathrm{e}^{L_F x_f}} - \dfrac{S_X}{S_F}\right\} S_F\,\mathrm{e}^{x-x_f}, & x < x_f \\ \\ T_{-\infty} + 1 + (\Delta T - 1)\mathrm{e}^{x} - \dfrac{T_a^2}{\theta}\left\{\dfrac{1-\mathrm{e}^{x}}{1-\mathrm{e}^{L_F x_f}}\right\} L_F S_F, & x > x_f, \end{cases}$$

$$Y \sim \begin{cases} 1 - \mathrm{e}^{L_F(x-x_f)} + \dfrac{T_a^2}{\theta}\left\{1 - \dfrac{L_F}{L_X}\dfrac{1-\mathrm{e}^{L_X x_f}}{1-\mathrm{e}^{L_F x^f}} + \dfrac{S_X}{S_F}\right\} L_F S_F\,\mathrm{e}^{L_F(x-x_f)}, & x < x_f \\ \\ \dfrac{T_a^2}{\theta}\left\{\dfrac{1-\mathrm{e}^{L_F x}}{1-\mathrm{e}^{L_F x_f}}\right\} L_F S_F, & x > x_f \end{cases}$$

$$X \sim \begin{cases} \dfrac{T_a^2}{\theta} L_X S_X\,\mathrm{e}^{L_X(x-x_f)}, & x < x_f \\ \\ (1+\phi^{-1})\mathrm{e}^{L_X x} - 1 + \dfrac{T_a^2}{\theta}\left\{\dfrac{1-\mathrm{e}^{L_X x}}{1-\mathrm{e}^{L_F x_f}}\right\} L_F S_F, & x > x_f, \end{cases}$$

with the location of the reaction sheet given by

$$x_f = -\ln\{(1+\phi^{-1})^{1/L_X}\}. \tag{5.6}$$

Note that x_f depends on the Lewis number of the reactant that diffuses against the stream. Thus, for the 'inverse' diffusion flame the location of the reaction sheet depends on L_F rather than L_X. The adiabatic flame temperature is given by

$$T_a = 1 + T_{-\infty} + (\Delta T - 1)(1+\phi^{-1})^{-1/L_X} \tag{5.7}$$

which agrees with (3.50) when $L_X = 1$.

The parameter γ takes the simple form

$$\gamma = -1 + 2(1+\Delta T)\left(\frac{\phi}{1+\phi}\right)^{1/L_X} \tag{5.8}$$

and is a measure of the mixture's strength in the reaction zone. Here too L_X is replaced by L_F for the 'inverse' diffusion flame. We recall that when $-1 < \gamma < 0$ more heat is transported to the fuel side and, consequently, the fuel is the more completely consumed reactant. When $0 < \gamma < 1$ on the other hand more heat is transported to the oxidant side and, consequently, the oxidant is the more completely consumed reactant. For unity Lewis numbers, and when the fuel and oxidant are supplied at the same temperature there is a simple relation between the parameter ϕ, which is based on the supply conditions, and γ which measures conditions at the reaction sheet. In this case $\gamma = (\phi - 1)/(\phi + 1)$ so that for $\phi < 1$, the fuel is the more completely consumed reactant, whereas for $\phi > 1$ the oxidant is the more completely consumed reactant. In general, however, γ depends on the rates at which heat and mass are transported to the reaction zone, namely on the temperature differential ΔT and on $L_X - 1$.

The leakage functions S_F and S_X are given by (3.45), (3.47), (3.46) and (3.48), respectively, where δ is determined by the relation (3.39) with h_F^* and h_X^* given by

$$\left.\begin{aligned} h_F^* &= -\left\{\frac{L_F(1-\mathrm{e}^{x_f})-(1-\mathrm{e}^{L_F x_f})}{1-\mathrm{e}^{L_F x_f}}\right\} S_F, \\ h_X^* &= -\frac{L_F}{L_X}\left\{\frac{L_X(1-\mathrm{e}^{x_f})-(1-\mathrm{e}^{L_X x_f})}{1-\mathrm{e}^{L_F x_f}}\right\} S_F. \end{aligned}\right\} \tag{5.9}$$

Note that for unity Lewis numbers the enthalpies $T+Y$ and $T+X$ are conserved scalars, in which case $h_F^* = h_X^* = 0$, as anticipated. Then, $\delta = 4L_F L_X D$ is fixed by the Damköhler number. For non-unity Lewis numbers h_i^* is positive/negative depending on whether L_i is less/greater than 1, respectively. The total enthaply $(1+\gamma)h_X^*/2 + (1-\gamma)h_F^*/2$, however, depends on both Lewis numbers and on the reactant leakages. The dependence of δ on D is therefore more complex.

5.2. *Linear stability analysis*

We introduce small disturbances $\sim \epsilon\,\theta^{-1}$, superimposed on the basic state, denoted here with subscript b, with $\epsilon \ll 1$. The disturbances are then resolved into normal modes so that the temperature and mass fractions are expressed in the form†

$$\left.\begin{aligned} T &= T_{\mathrm{b}}(x) + \epsilon\ \theta^{-1}\,\tau(x)\ \exp(\mathrm{i}k_1 y + \mathrm{i}k_2 z + \sigma t) + \cdots, \\ Y &= Y_{\mathrm{b}}(x) + \epsilon\,\theta^{-1}\,\eta(x)\ \exp(\mathrm{i}k_1 y + \mathrm{i}k_2 z + \sigma t) + \cdots, \\ X &= X_{\mathrm{b}}(x) + \epsilon\,\theta^{-1}\,\xi(x)\ \exp(\mathrm{i}k_1 y + \mathrm{i}k_2 z + \sigma t) + \cdots, \end{aligned}\right\} \tag{5.10}$$

with the location of the reaction sheet given by

$$x = x_f + \epsilon\,\theta^{-1} A \exp(\mathrm{i}k_1 y + \mathrm{i}k_2 z + \sigma t).$$

Here ϵA is the (small) amplitude, k_1 and k_2 are the wavenumbers in the y- and z-directions, respectively, and σ is a complex number whose real part identifies the growth rate of the disturbance. Substituting into the governing equations (5.3)–(5.5), one finds

$$\frac{\mathrm{d}^2\tau}{\mathrm{d}x^2} - \frac{\mathrm{d}\tau}{\mathrm{d}x} - (\sigma + k^2)\tau = 0,$$

$$\frac{\mathrm{d}^2\eta}{\mathrm{d}x^2} - L_F\frac{\mathrm{d}\eta}{\mathrm{d}x} - (L_F\sigma + k^2)\eta = 0,$$

$$\frac{\mathrm{d}^2\xi}{\mathrm{d}x^2} - L_X\frac{\mathrm{d}\xi}{\mathrm{d}x} - (L_X\sigma + k^2)\xi = 0,$$

where $k = (k_1^2 + k_2^2)^{1/2}$ is the total wavenumber. Solutions, which vanish at $x = 0$ and

† No confusion is caused by using here symbols that were used previously in analysing the reaction zone structure.

as $x \to -\infty$, are

$$\tau = \begin{cases} C_1 \exp[(\tfrac{1}{2} + \lambda_T)x], & x < x_f \\ D_1\{\exp[(\tfrac{1}{2} + \lambda_T)x] - \exp[(\tfrac{1}{2} - \lambda_T)x]\}, & x > x_f, \end{cases}$$

$$\eta = \begin{cases} C_2 \exp[(\tfrac{1}{2}L_F + \lambda_F)x], & x < x_f \\ D_2\{\exp[(\tfrac{1}{2}L_F + \lambda_F)x] - \exp[(\tfrac{1}{2}L_F - \lambda_F)x]\}, & x > x_f, \end{cases}$$

$$\xi = \begin{cases} C_3 \exp[(\tfrac{1}{2}L_X + \lambda_X)x], & x < x_f \\ D_3\{\exp[(\tfrac{1}{2}L_X + \lambda_X)x] - \exp[(\tfrac{1}{2}L_X - \lambda_X)x]\}, & x > x_f, \end{cases}$$

where

$$\lambda_j = \tfrac{1}{2}\sqrt{L_j^2 + 4(L_j\sigma + k^2)}, \qquad j = T, F, X,$$

with $L_T \equiv 1$. Because of our interest in identifying unstable solutions, we have restricted attention to modes corresponding to $\mathrm{Re}(\sigma) > 0$, a condition that has been used in discarding the exponentially growing solutions for large negative x.

The jump relationships (4.7)–(4.8) yield

$$[\tau] = -L_F^{-1}[\eta] = -L_X^{-1}[\xi],$$

$$\left[\tau - \frac{\mathrm{d}\tau}{\mathrm{d}x}\right] = -\left[\eta - L_F^{-1}\frac{\mathrm{d}\eta}{\mathrm{d}x}\right] = -\left[\xi - L_X^{-1}\frac{\mathrm{d}\xi}{\mathrm{d}x}\right],$$

to be satisfied across $x = x_f$. Thus

$$\tau^+ - \tau^- + L_F^{-1}\eta_f^+ - L_F^{-1}\eta_f^- = 0, \tag{5.11}$$

$$\tau^+ - \tau^- + L_x^{-1}\xi_f^+ - L_x^{-1}\xi_f^- = 0, \tag{5.12}$$

$$a_T\,\tau^+ + (\tfrac{1}{2} - \lambda_T)\tau^- + a_F\,\eta^+ + (\tfrac{1}{2} - L_F^{-1}\lambda_F)\,\eta^- = 0, \tag{5.13}$$

$$a_T\,\tau^+ + (\tfrac{1}{2} - \lambda_T)\tau^- + a_X\,\xi^+ + (\tfrac{1}{2} - L_X^{-1}\lambda_X)\,\xi^- = 0, \tag{5.14}$$

with the superscripts $\pm$ denoting conditions at $x = x_f^{\pm}$, respectively, and where

$$a_j = \frac{1}{L_j}\frac{(\tfrac{1}{2}L_j + \lambda_j)\exp[-\lambda_j x_f] - (\tfrac{1}{2}L_j - \lambda_j)\exp[\lambda_j x_f]}{\exp[\lambda_j x_f] - \exp[-\lambda_j x_f]}, \qquad j = T, F, X.$$

It thus remains to apply conditions (4.13). The expansions (5.10) imply that δ can also be written as

$$\delta \sim \delta_{\mathrm{b}} + \epsilon\hat{\delta}\exp(\mathrm{i}k_1 y + \mathrm{i}k_2 z + \sigma t)$$

with

$$\delta_{\mathrm{b}} = 4L_F L_X D \exp\left\{\frac{1+\gamma}{2}(h_X^*)_{\mathrm{b}} + \frac{1-\gamma}{2}(h_F^*)_{\mathrm{b}}\right\}.$$

The exponent in (3.39) takes the form

$$\frac{1+\gamma}{2}(h_X^*)_{\mathrm{b}} + \frac{1-\gamma}{2}(h_F^*)_{\mathrm{b}} + \epsilon\left\{\frac{1+\gamma}{2}(\tau^- + L_X^{-1}\xi^-) + \frac{1-\gamma}{2}(\tau^+ + L_F^{-1}\eta^+)\right\}\exp(\mathrm{i}k_1 y + \mathrm{i}k_2 z + \sigma t)$$

where $(h_X^*)_\mathrm{b}$ and $(h_F^*)_\mathrm{b}$ are given by (5.9). Upon linearization one finds

$$\hat{\delta} = \delta_\mathrm{b}\left\{\frac{1+\gamma}{2}(\tau^- + L_X^{-1}\xi^-) + \frac{1-\gamma}{2}(\tau^+ + L_F^{-1}\eta^+)\right\}.$$

Now, expanding the functions S_F and S_X for $\epsilon \ll 1$, we have

$$S_F = S_F(\gamma,\delta_\mathrm{b}) + \epsilon\,\frac{\partial S_F}{\partial\delta}(\gamma,\delta_\mathrm{b})\hat{\delta}\exp(\mathrm{i}k_1 y + \mathrm{i}k_2 z + \sigma t) + \cdots,$$

$$S_X = S_X(\gamma,\delta_\mathrm{b}) + \epsilon\,\frac{\partial S_X}{\partial\delta}(\gamma,\delta_\mathrm{b})\hat{\delta}\exp(\mathrm{i}k_1 y + \mathrm{i}k_2 z + \sigma t) + \cdots,$$

so that the disturbance in the fuel and oxidant leakages

$$\eta^+ = L_F\frac{\partial S_F}{\partial\delta}(\gamma,\delta_\mathrm{b})\hat{\delta}, \qquad \xi^- = L_X\frac{\partial S_X}{\partial\delta}(\gamma,\delta_\mathrm{b})\hat{\delta},$$

are expressed in terms of the leakage functions $S_F(\gamma,\delta_\mathrm{b})$ and $S_X(\gamma,\delta_\mathrm{b})$ of the basic state. We thus find that

$$\frac{1-\gamma}{2}L_F\,b_F\,\tau^+ + \frac{1+\gamma}{2}L_F\,b_F\,\tau^- + \left(\frac{1-\gamma}{2}b_F - 1\right)\eta^+ + \frac{L_F}{L_X}\frac{1+\gamma}{2}b_F\xi^- = 0, \quad (5.15)$$

$$\frac{1-\gamma}{2}L_X\,b_X\,\tau^+ + \frac{1+\gamma}{2}L_X\,b_X\,\tau^- + \frac{L_X}{L_F}\frac{1-\gamma}{2}b_X\,\eta^+ + \left(\frac{1+\gamma}{2}b_X - 1\right)\xi^- = 0, \quad (5.16)$$

where

$$b_j = \delta_\mathrm{b}\,\frac{\partial S_j}{\partial\delta}(\gamma,\delta_\mathrm{b}), \qquad j = F, X.$$

The six relations (5.11)–(5.16) form a homogeneous linear system which has non-trivial solutions if and only if

$$\begin{Vmatrix}
1 & -1 & L_F^{-1} & -L_F^{-1} & 0 & 0 \\
1 & -1 & 0 & 0 & L_X^{-1} & -L_X^{-1} \\
a_T & \frac{1}{2}-\lambda_T & a_F & \frac{1}{2}-L_F^{-1}\lambda_F & 0 & 0 \\
a_T & \frac{1}{2}-\lambda_T & 0 & 0 & a_X & \frac{1}{2}-L_X^{-1}\lambda_X \\
\frac{1-\gamma}{2}L_F b_F & \frac{1+\gamma}{2}L_F\,b_F & \frac{1-\gamma}{2}b_F - 1 & 0 & 0 & \frac{L_F}{L_X}\frac{1+\gamma}{2}b_F \\
\frac{1-\gamma}{2}L_X b_X & \frac{1+\gamma}{2}L_X\,b_X & \frac{L_X}{L_F}\frac{1-\gamma}{2}b_X & 0 & 0 & \frac{1+\gamma}{2}b_X - 1
\end{Vmatrix} = 0.$$

This solvability condition is the dispersion relation that relates the growth rate σ to the remaining parameters: the wavenumber k, the Damköhler number D, the Lewis numbers L_F and L_X, the mixture's strength ϕ and the temperature differential ΔT. It takes the form

$$\delta_\mathrm{b}\frac{\partial S_F}{\partial\delta_\mathrm{b}}\left\{\frac{1-\gamma}{2}\frac{[\lambda_F\coth(\lambda_F x_f) - \lambda_X\coth(\lambda_X x_f)] - \frac{1}{2}(L_F - L_X)}{[\lambda_F - \lambda_F\coth(\lambda_F x_f)][\lambda_X - \lambda_X\coth(\lambda_X x_f)]}\right.$$

$$\left. + \frac{[\lambda_X\coth(\lambda_X x_f) - \lambda_T\coth(\lambda_T x_f)] - \frac{1}{2}(L_X - 1)}{[\lambda_X - \lambda_X\coth(\lambda_X x_f)][\lambda_T - \lambda_T\coth(\lambda_T x_f)]}\right\}$$

$$+\delta_b\frac{\partial S_X}{\partial\delta_b}\left\{\frac{1+\gamma}{2}\frac{(\lambda_F-\lambda_X)-\frac{1}{2}(L_F-L_X)}{[\lambda_F-\lambda_F\coth(\lambda_F x_f)][\lambda_X-\lambda_X\coth(\lambda_X x_f)]}\right.$$

$$\left.+\frac{(\lambda_T-\lambda_F)-\frac{1}{2}(1-L_F)}{[\lambda_T-\lambda_T\coth(\lambda_T x_f)][\lambda_F-\lambda_F\coth(\lambda_F x_f)]}\right\}$$

$$-\left\{\frac{[\lambda_F-\lambda_X\coth(\lambda_X x_f)]-\frac{1}{2}(L_F-L_X)}{[\lambda_X-\lambda_X\coth(\lambda_X x_f)][\lambda_F-\lambda_F\coth(\lambda_F x_f)]}\right\}=0. \tag{5.17}$$

Generally, solutions of this transcendental equation must be found numerically. Before discussing the numerical results we examine some special limits.

We first consider the limit $D\to\infty$ corresponding to complete combustion – the 'Burke–Schumann' limit. In this case $S_F, S_X\to 0$ and the dispersion relation simplifies to

$$\tanh(\lambda_X x_f)=\frac{2\lambda_X}{L_X+(2\lambda_F-L_F)}.$$

For real values of σ the left-hand side is negative, since $x_f<0$, while the right-hand side is always positive. There are no solutions to the dispersion relation with σ real. When σ is complex, by decomposing the dispersion relation into its real and imaginary parts, it can likewise be verified that no solutions with $\mathrm{Re}(\sigma)>0$ exist. We conclude that, for all values of the Lewis numbers, there are no unstable modes in the limit $D\to\infty$. *The Burke–Schumann flame sheet is therefore unconditionally stable* to small disturbances.

When the Lewis numbers are both equal, and equal to 1, the left-hand side of (5.17) reduces to $-[\lambda_T(1-\coth(\lambda_T x_f)]^{-1}$ which is strictly negative for all k so that the dispersion relation can never be satisfied. We conclude that *when the thermal and mass diffusivities are all equal, the flame is unconditionally stable* to small disturbances.†

5.3. *Cellular instability*

In the following we will be only concerned with *real* values of the growth rate σ. Thus, at an instability threshold the bifurcation is steady and describes the onset of cellular flames. The occurrence of a Hopf bifurcation with $\mathrm{Im}(\sigma)\neq 0$ at the instability threshold, associated with the onset of pulsating flames and/or travelling waves along the flame front, will be discussed in a future publication. Consequently, we restrict attention here to Lewis numbers that are less than or equal to 1, i.e. $L_F\leqslant 1$ and $L_X\leqslant 1$, disregarding the case $L_F=L_X=1$ which has been already discussed above.

It is instructive to examine the dispersion relation in the limit $k\to\infty$ with $\sigma=O(1)$. Since $\lambda_j\sim k$, we find that

$$\frac{1}{4}\left\{\delta_b\frac{\partial S_F}{\partial\delta_b}-\delta_b\frac{\partial S_X}{\partial\delta_b}\right\}\left\{\frac{1-\gamma}{2}(1-L_F)+\frac{1+\gamma}{2}(1-L_X)\right\}+\tfrac{1}{4}(L_F-L_X)\sim k.$$

A balance between the left- and right-hand sides can be achieved near the turning point $\delta\approx\delta_c$, where the slopes $\partial S_F/\partial\delta_b$ and/or $\partial S_X/\partial\delta_b$ become large, or at large δ on the upper branch of the response curve. In particular, such a balance is not possible for states corresponding to the lower branch of the response curve, remote from $\delta=\delta_c$. Thus, for sufficiently large values of δ, steady states on the lower branch

† This holds as long as S_F (or S_X) are $O(1)$ quantities and therefore excludes states on the upper branch of the S_F,δ curve that are sufficiently far from δ_c. Such states are of no physical interest.

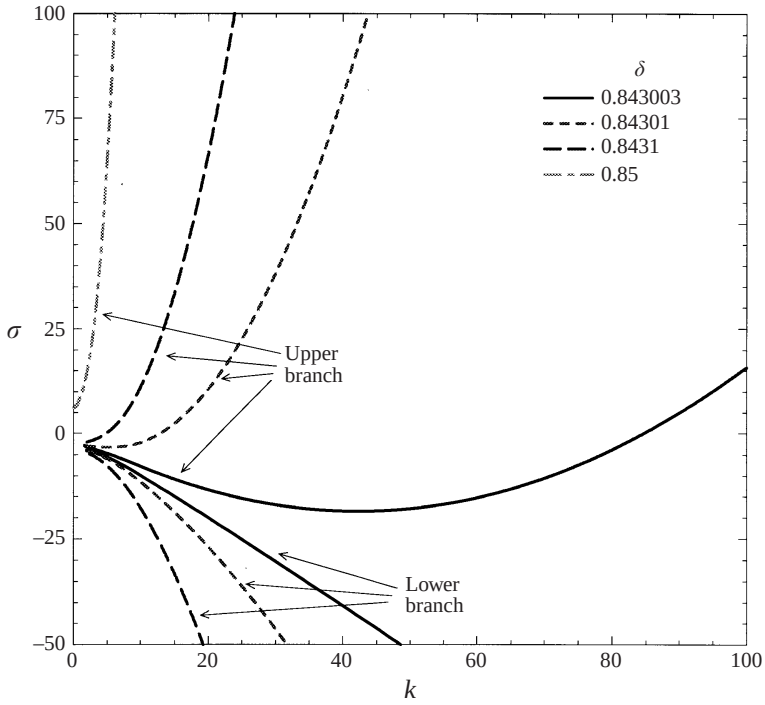

FIGURE 8. The dependence of the growth rate on the wavenumber, for $L_F = 0.5$, $L_X = 1.0$, and $\phi = 2$ ($\gamma = 1/3$, $\delta_c = 0.84300296$).

of the response curve are stable to short-wavelength disturbances. Near the turning point, however, unstable modes corresponding to large k are possible, with results sensitive to the value of γ. For values of γ sufficiently positive, $|\partial S_X/\partial\delta_b| \ll |\partial S_F/\partial\delta_b|$ which implies that

$$k \sim \tfrac{1}{4}\delta_b \frac{\partial S_F}{\partial \delta_b}\left\{\frac{1-\gamma}{2}(1-L_F)+\frac{1+\gamma}{2}(1-L_X)\right\}. \tag{5.18}$$

Thus, unstable modes with large k can be found on the upper branch of the response curve, where $\partial S_F/\partial\delta_b > 0$. For values of γ sufficiently negative, $|\partial S_F/\partial\delta_b| \ll |\partial S_X/\partial\delta_b|$ so that

$$k \sim -\tfrac{1}{4}\delta_b \frac{\partial S_X}{\partial \delta_b}\left\{\frac{1-\gamma}{2}(1-L_F)+\frac{1+\gamma}{2}(1-L_X)\right\}. \tag{5.19}$$

Now, unstable modes with large k can also be found on the lower branch of the response curve, where $\partial S_X/\partial\delta_b < 0$.

Numerical solutions of the full dispersion relation (5.17) for values of δ_b near δ_c confirm these assertions. In figures 8 and 9 the dependence of σ on k is shown for the same values of the Lewis numbers and δ_b, but for values of γ of opposite sign. In figure 8 one sees that for $\gamma > 0$, solutions on the lower branch of the response curve are stable and those on the upper branch are always unstable. As $\delta_b \to \delta_c$ from the upper branch, this instability corresponds to large k, as suggested by (5.18); long-wavelength disturbances (small k) are in fact stable. Note also from figure 8 that the instability on the upper branch, for $\delta_b - \delta_c < 10^{-6}$, occurs for large but finite k suggesting that, as $\delta_b \to \delta_c$, the exchange of stability may in fact correspond

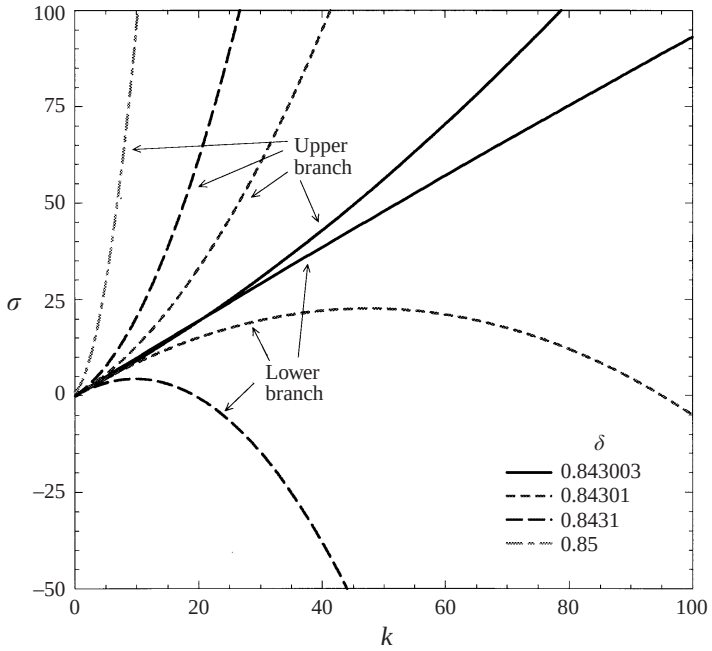

FIGURE 9. The dependence of the growth rate on the wavenumber, for $L_F = 0.5$, $L_X = 1.0$, and $\phi = 0.5$ ($\gamma = -1/3$, $\delta_c = 0.84300296$).

to $k \to \infty$. In figure 9, one sees that for $\gamma < 0$, solutions on the upper branch are always unstable with $\sigma \to \infty$ as $k \to \infty$. Here, however, solutions on the lower branch are also unstable: the associated growth rates increase with increasing k, reach a maximum, and then decrease, becoming negative for $k > k_{\max}$. As $\delta_b \to \delta_c$ from the lower branch, the range of unstable modes widens and $k_{\max}$ becomes exceedingly large, as suggested by (5.19). It is clear from the dependence of σ on k revealed in figure 9 that for $\gamma < 0$ the onset of instability occurs at some value of δ_b on the lower branch, sufficiently far from δ_c, but not too far, since we have shown that the steady states are unconditionally stable as $\delta_b \to \infty$.

We remarked earlier that, away from the turning point, the dispersion relation implies that steady states on the lower branch of the response curve are stable to short-wavelength disturbances and the numerical calculations corroborate the lack of a short-wavelength instability for δ sufficiently far from δ_c. This suggests that for $\gamma < 0$ the onset instability occurs at some value of δ_b on the lower branch of the response curve and that such instabilities correspond to $O(1)$ values of k. As γ is increased the critical δ_b corresponding to the onset of instability moves toward δ_c, and the wavenumber at onset of instability increases, becoming large as γ becomes positive.

So far we have been referring to the 'response curve' as the curve that illustrates the dependence of the basic state, characterized for example by the leakage of one of the reactants, on δ_b (which appears quite naturally in the analysis). Since the Damköhler number is the physically controllable parameter, it is more appropriate to illustrate the dependence of the solution on D so that for fixed values of the remaining parameters the response curve identifies the state corresponding to a given D. Burning states correspond to $D_{ex} < D < \infty$. We recall, however, that the dependence of δ on

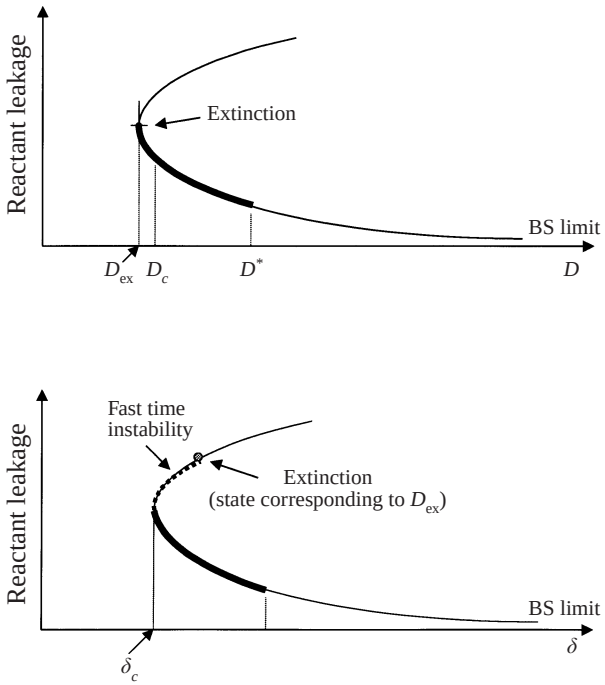

FIGURE 10. Response curves plotted against the parameter δ and against the Damköhler number D identifying in each the states corresponding to extinction and to marginal stability.

D is in general nonlinear so that δ_c and $D_{\rm ex}$ do not represent the same physical state. Depending on the Lewis numbers, δ_c may correspond to a state $D = D_c$ on the upper or lower branch of the response curve drawn against D. In particular, it appears that for Lewis numbers less than 1, as considered here, the state corresponding to δ_c is a state on the lower branch of the response curve, namely $D_c > D_{\rm ex}$ as illustrated in figure 10. Thus, the steady states corresponding to $D_{\rm ex} < D < D_c$ are solutions on the upper branch of the $S_F, \delta_{\rm b}$ curve and, according to the results of figures 8 and 9, are unstable. Furthermore, the unstable modes extend to sufficiently large values of k and the associated growth rates σ are quite large. Such disturbances therefore evolve on a relatively 'fast time'. This behaviour is consistent with the results of Kim *et al.* (1996) who re-examined the problem by re-scaling time on the reaction zone thickness in order to determine the wavenumber corresponding to maximum growth rate. However, unlike their conclusion that the marginal stability state is that corresponding to D_c, we identify here unstable modes for $D > D_c$ that evolve on the (ordinary) diffusion time scale. Figure 11, for example, shows the dependence of the growth rate σ on k for $D > D_c$. We note that for sufficiently large D the growth rate $\sigma < 0$, implying stability. Furthermore, for $D < D^*$ say, there is a limited range of growing modes with the maximum growth rate corresponding to $k_{\rm max} \sim 1$–2. As $D \to D_c$ the growth rate as well as $k_{\rm max}$ become large, in accord with our previous conclusions.

We have thus seen that by reducing the Damköhler number, starting from large values, a point is reached below which the planar flame becomes unstable. The critical point, corresponding to $D = D^*$, identifies the onset of a cellular flame, with distinct cell size $\sim 2\pi/k_{\rm max}$. We shall now examine the dependence of the marginal states on the Lewis numbers and mixture strength. For simplicity, we assume equal fuel

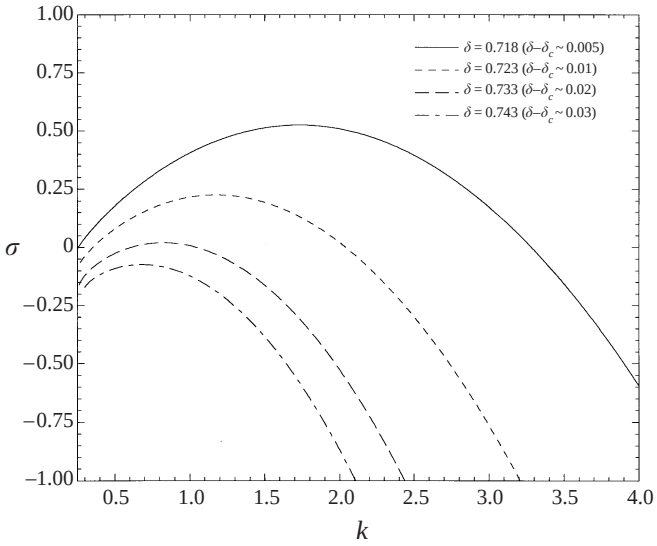

FIGURE 11. The growth rate σ as a function the wavenumber k for selected values of δ corresponding to $D > D_c$. Calculated for $L_F = L_X = 0.5, \phi = 0.833333, \gamma = -0.586777$.

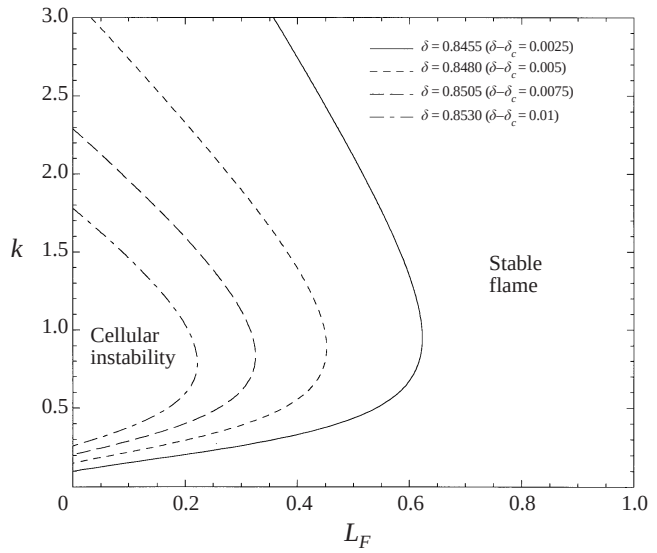

FIGURE 12. Stability curves showing regions of stability/instability in the parameter plane of L_F versus k. Calculated for $L_X = 1.0$, and $\phi = 0.5$ ($\gamma = -1/3$, $\delta_c = 0.84300$).

and oxidant supply temperatures, i.e. $\Delta T = 0$. The results are based on numerical solutions of the transcendental equation (5.17).

We found that cellular instability results when the reactant supplied in the feed stream (here the fuel) is the more completely consumed reactant ($\gamma < 0$), and the corresponding Lewis number is sufficiently small ($L_F < L_F^*$). Figure 12 shows marginal stability curves ($\sigma = 0$) in the parameter plane L_F vs. k for $L_X = 1$ and $\phi = 0.5$. The different curves correspond to different values of δ. For a given value of L_F, the unstable modes are restricted to a finite range of wavelengths, provided $L_F < L_F^*$. As

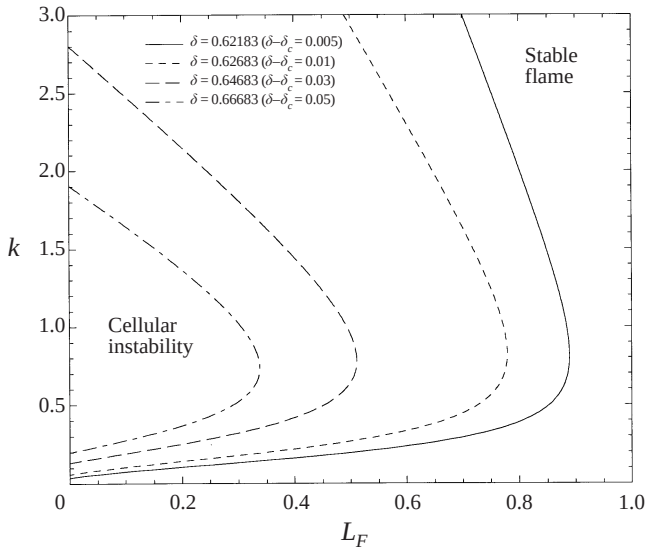

FIGURE 13. Stability curves showing regions of stability/instability in the parameter plane of L_F versus k. Calculated for $L_X = 0.6$, and $\phi = 0.5$ ($\gamma = -0.67950$, $\delta_c = 0.61683$).

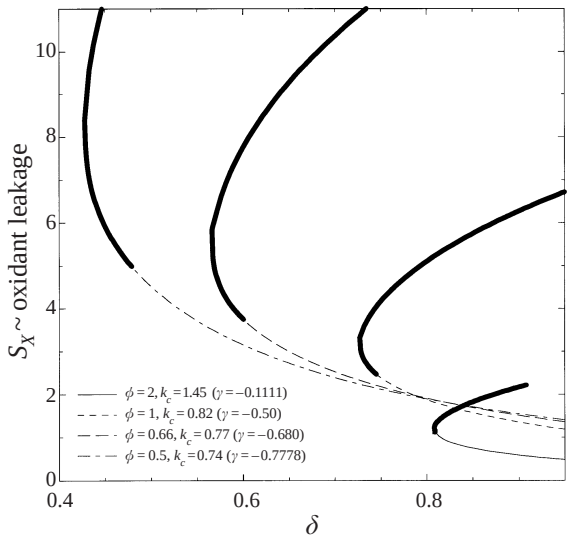

FIGURE 14. Response curves of $S_X \sim$ oxidant leakage versus δ, for $L_X = L_F = 0.5$ and several values of the oxidant source mass fraction ϕ. Darkened portions of the response curves correspond to unstable states.

δ approaches δ_c, this range increases, as does the range of the fuel Lewis numbers over which instability may be found. Figure 13 shows similar curves but for $L_X = 0.6$. The comparison shows that cellular instability is more accessible when the Lewis number of the oxidant L_X is lowered; it results for a larger range of both L_F and δ. Thus, there exists a critical oxidant Lewis number L_X^* above which no instability can be found. The two critical values L_F^* and L_X^* are inversely related. Finally we note that, as $\delta \to \delta_c$, the range of unstable modes extends to large wavenumbers.

The dependence of the instability on the parameter ϕ is illustrated in figure 14.

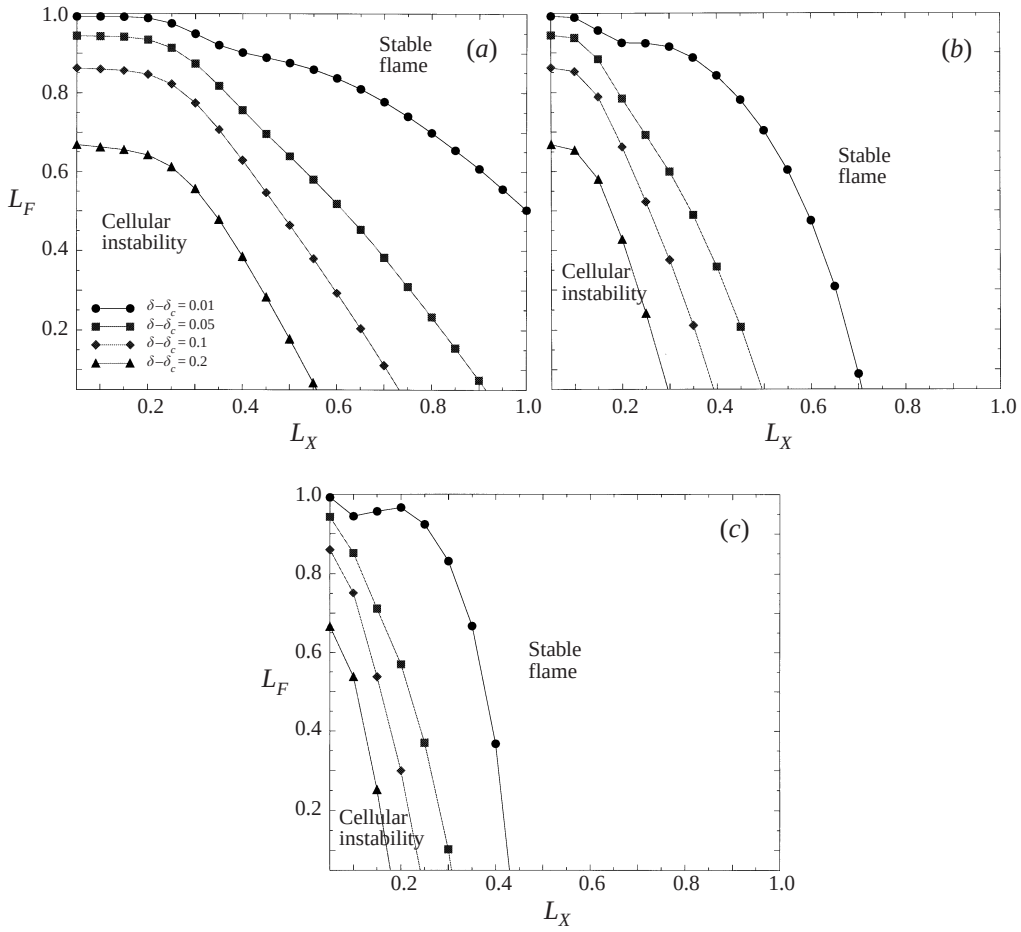

FIGURE 15. Regions of stability/instability in the parameter plane L_F, L_X, calculated for several values of $\delta - \delta_c$ and (*a*) $\phi = 1/3$, (*b*) $\phi = 1.0$, (*c*) $\phi = 2.0$.

Here response curves of the oxidant leakage S_X versus δ are shown for several values of ϕ. The darkened segments of the response curves correspond to unstable states. As ϕ is decreased, the parameter γ decreases, signifying that the fuel is becoming more deficient in the reaction zone, and instability is found over a greater range of δ. The critical wavenumber k_c increases with increasing ϕ.

Figures 15(*a–c*) shows curves in the parameter plane L_F versus L_X that separate regions where the planar flame is stable from regions where a cellular instability results. The different curves correspond to different values of δ, and the different graphs to different values of ϕ. The closer δ is to δ_c the wider the range of Lewis numbers for which cellular instability results. This range, however, shrinks as ϕ increases. Thus, cellular flames are more likely to occur when ϕ is small, namely when the fuel stream is sufficiently diluted. Consistent with our earlier predictions, the figures show that the flame is stable when both Lewis numbers are equal to 1.

5.4. *Discussion*

As in premixed systems, the disparity between the thermal diffusivity of the mixture and the molecular diffusivities of the reactants is responsible for the development of

cellular diffusion flames. The situation in non-premixed systems, however, is somewhat more complex. When the Damköhler number is sufficiently large, corresponding to a short chemical reaction time or fast chemistry, combustion occurs almost instantaneously and is therefore constrained to the stoichiometric surface – the surface where fuel and oxidant meet in stoichiometric proportions. The fuel and oxidant are completely consumed and the reaction sheet separates a region of fuel but no oxidant from a region where there is only oxidant. Since complete combustion, dictated by the short chemical reaction time, can only occur along the stoichiometric surface any slight disturbance of the reaction sheet is obliterated and the planar flame is stable. For smaller values of the Damköhler number there is incomplete combustion with significant reactants leakage. The degree of fuel and oxidant consumption in this case depends strongly on their transport to the reaction sheet, and therefore on the Lewis numbers. While thermal diffusion tends to nullify temperature differences, and hence has a stabilizing influence, molecular diffusivity may enhance these differences. For Lewis numbers less than 1, molecular diffusivity is larger than the thermal diffusivity and therefore plays a more important role. Furthermore, the reactant supplied in the feed stream – the fuel in the configuration examined here (see figure 7) – plays a more significant role than the reactant diffusing against the stream. Now, consider the situation in which the reaction sheet is slightly corrugated. Near segments of the wrinkled sheet convex towards the fuel region the isotherms on the fuel side are more dense while on the oxidant side they spread out. Consequently, the oxidant leakage through the reaction sheet increases providing the necessary oxidant concentration for the reaction to proceed, thus overcoming its natural tendency to revert to the stoichiometric surface. Under these conditions the more natural mode of burning is therefore along a cellular reaction sheet.

We have shown that cellular instability results in diffusion flames only for near extinction conditions, namely when there is significant reactant leakage through the reaction zone. Experiments likewise indicate that the onset of cellularity is usually associated with high flow rates (Garside & Jackson 1953; Dongworth & Melvin 1976) or near-extinction conditions (Ishizuka & Tsuji 1981; Chen *et al.* 1992), namely for low values of the Damköhler number D. Furthermore, the instability results when the reactant supplied in the feed stream (here the fuel) is the more completely consumed reactant and the corresponding Lewis number (here L_F) is sufficiently small, in other words when $S_F < S_X$ (or $\gamma < 0$) and $L_F < L_F^*$. The experimental results reported by Dongworth & Melvin (1976), Ishizuka & Tsuji (1981) and Chen *et al.* (1992) indicate that cellular flames were observed for an H_2–O_2 flame when the hydrogen was diluted in nitrogen or argon; in these cases $L_F \sim 0.35$–0.33 is sufficiently low. Cellularity was not observed when the diluent was helium, in which case $L_F \sim 1.02$ is too large.

We have also shown that for a diffusion flame to exhibit cellular instability both Lewis numbers must be below critical values, namely $L_F < L_F^*$, $L_X < L_X^*$. Recall that we have limited the discussion to Lewis numbers less than 1 so that it may be possible for an instability to exist when L_X exceeds 1 if L_F is sufficiently low, or when L_F exceeds 1 if L_X is sufficiently low. The stability/instability regions mapped in the Lewis numbers parameter plane (figure 15) are in complete agreement with the careful account of flame behaviour given in Chen *et al.* (1992). It was reported there that a methane–oxygen flame diluted in He or N_2 ($L_F = 1.83, 0.96$ and $L_X = 1.64, 1.01$ respectively) did not exhibit cellularity, but it did when diluted in SF_6 ($L_F = 0.39$ and $L_X = 0.48$). Similarly a propane–oxygen flame diluted in N_2 and CO_2 ($L_F = 1.79, 1.39$ and $L_X = 0.99, 0.80$ respectively) did not exhibit cellularity but it did when diluted in SF_6 ($L_F = 0.70$ and $L_X = 0.53$).

One notes from (5.8) that for $\Delta T = 0$ the parameter γ decreases both as ϕ or L_X decreases. As γ decreases, there is more oxidant and less fuel leakage through the reaction zone, which suggests that the flame becomes more and more susceptible to cellularity when ϕ is reduced. This trend, which can be also detected from the stability diagrams, is in agreement with the observations reported by Chen *et al.* (1992). A hydrogen–oxygen flame diluted with nitrogen was non-cellular with $\phi = 2$, but became cellular when ϕ was reduced to 1.

The fastest growing mode, which would become the dominant one beyond the instability threshold, is indicative of the dimension of the cells that develop on the flame. The (dimensional) critical wavelength is $2\pi\ell_D/k_{\max}$. Our results show that $k_{\max} \sim 0.7$–1.4 which implies that with a thermal diffusivity $\sim 0.22\,\mathrm{cm^2\,s^{-1}}$ and velocities $U \sim 1$–$2\,\mathrm{cm\,s^{-1}}$ (typical normal velocity component estimated from the various experimental set-ups) the predicted cells are ~ 0.5–2 cm, which is within the observed range. A more direct comparison would require more accurate knowledge of the characteristic velocity U, for the determination of the diffusion length ℓ_D and of the Damköhler number D, for the determination of $k_{\max}$. Neither one could be obtained with sufficient accuracy that would improve the above estimate.

As alluded to earlier, the results discussed here are contingent on the fuel being provided in the feed stream, in which case the net mass flux is directed from the fuel side towards the oxidant side. The results of the equivalent but opposite problem, in which the oxidant is supplied in the feeding stream, are obtained by interchanging the role of F and X in the solution. Instability in this case would occur for rich flames. The result that cellularity is associated with a lean flame is consistent with the splitter-plate experiment of Dongworth & Melvin (1976) who hypothesized that cellularity was peculiar to lean (fuel deficient) flames. Our prediction that cellularity could also result in rich flames is contingent upon having an oxidant with sufficiently low Lewis number. These however are seldom found, which may explain why cellular flames under rich conditions were not observed.

This work has been partially supported by the National Science Foundation under grants DMS9703716 and CTS9521022. Some of this work was performed while S. Cheatham held a National Research Council-Naval Research Laboratory Research Associateship.

REFERENCES

Ascher, U. Christiansen, J. & Russell, R. D. 1981 *COLSYS: Collocation Software for Boundary Value ODE's*. ACM Transaction on Mathematical Software, vol. 7, pp. 209–222.

Buckmaster, J. & Ludford, G. S. S. 1982 *Theory of Laminar Flames*. Cambridge University Press.

Buckmaster, J., Nachman, A. & Taliaferro, S. 1983 The fast-time instability of diffusion flames. *Physica* **9D**, 408–424.

Buckmaster, J. D. & Short, M. 1999 Cellular instabilities, sublimit structures and edge-flames in premixed counterflows. *Combust. Theory Modelling* **3**, 199–214.

Burke, S. P. & Schumann, T. E. W. 1928 Diffusion flames. *Indust. Engng Chem.* **20**, 998–1004.

Cheatham, S. 1997 On the structure and stability of diffusion flames. PhD thesis, Northwestern University.

Cheatham, S. & Matalon, M. 1996*a* Near-limit oscillations of spherical diffusion flames. *AIAA J.* **34**, 1403–1409.

Cheatham, S. & Matalon, M. 1996*b* Heat loss and Lewis number effects on the onset of oscillations in diffusion flames. *Twenty-Sixth Symp. (Intl) on Combustion*, pp. 1063–1070. The Combustion Institute, Pittsburgh.

Chen, R., Mitchell, G. B. & Ronney, P. D. 1992 Diffusive-thermal instability and flame extinction

in nonpremixed combustion. *Twenty-Fourth Symp.* (*Intl*) *on Combustion*, pp. 213–221. The Combustion Institute, Pittsburgh.

Chung, S. H. & Law, C. K. 1983 Structure and extinction of convective diffusion flames with general Lewis numbers. *Combust. Flame* **52**, 59–79.

Dongworth, M. R. & Melvin, A. 1976 The transition to instability in a steady hydrogen–oxygen diffusion flame. *Combust. Sci. Technol.* **14**, 177–182.

Fischer, I., Buckmaster, J., Lozinski, D. & Matalon, M. 1994 Vapor diffusion flames, their stability, and annular pool fires. In *Modeling in Combustion Science*, pp. 249–257. Springer.

Gardside, J. E. & Jackson, B. 1951 Polyhedral diffusion flames. *Nature* **168**, 1085.

Gardside, J. E. & Jackson, B. 1953 The formation and some properties of polyhedral burner flames. *Fourth Symp.* (*Intl*) *on Combustion*, pp. 545–552. The Combustion Institute, Pittsburgh.

Ida, M. P. & Miksis, M. J. 1998 The dynamics of thin films I: General theory. *SIAM J. Appl. Maths* **58**, 456–473.

Ishizuka, S. & Tsuji, H. 1981 An experimental study of effect of inert gases on extinction of laminar diffusion flames. *Eighteenth Symp.* (*Intl*) *on Combustion*, pp. 695–703. The Combustion Institute, Pittsburgh.

Kim, J. S. 1997 Linear analysis of diffusional-thermal instability in diffusion flames with Lewis numbers close to unity. *Combust. Theory Modeling* **1**, 13–40.

Kim, J. S. & Williams, F. A. 1997 Extinction of diffusion flames with nonunity Lewis numbers. *J. Engng Maths* **31**, 101–118.

Kim, J. S., Williams, F. A. & Ronney, P. D. 1996 Diffusional–thermal instability of diffusion flames. *J. Fluid Mech.* **327**, 273–301.

Kirkby, L. L. & Schmitz, R. A. 1966 An analytical study of the stability of a laminar diffusion flame. *Combust. Flame* **10**, 205–220.

Linan, A. 1974 The asymptotic structure of counterflow diffusion flames for large activation energies. *Acta Astronautica* **1**, 1007–1039.

Linan, A. & Williams, F. A. 1993 *Fundamental Aspects of Combustion*. Oxford.

Matalon, M. & Ludford, G. S. S. 1980 On the near-ignition stability of diffusion flames. *Intl J. Engng Sci.* **18**, 1017–1026.

Matalon, M. & Matkowsky, B. J. 1982 Flames as gasdynamic discontinuities. *J. Fluid Mech.* **124**, 239–259.

Matalon, M. & Matkowsky, B. J. 1983 Flames in fluids: Their interactions and stability. *Combust. Sci. Technol.* **34**, 295–316.

Mills, K. & Matalon, M. 1997 Burner-generated spherical diffusion flames. *Combust. Sci. Technol.* **129**, 295–319.

Mills, K. & Matalon, M. 1998 Extinction of spherical diffusion flames in the presence of radiant loss. *Twenty-Seventh Symp.* (*Intl*) *on Combustion*, pp. 2535–2541. The Combustion Institute, Pittsburgh.

Peters, N. 1978 On the stability of linan's premixed flame regime. *Combust. Flame*, **33**, 315–318.

Peters, N. 1983 Local quenching due to flame stretch and non-premixed turbulent combustion. *Combust. Sci. Technol.* **30**, 1–17.

Peters, N. 1986 Laminar flamelet concept in turbulent combustion. *Twenty-First Symp.* (*Intl*) *on Combustion*, pp. 1231–1250. The Combustion Institute, Pittsburgh.

Rosenhead, L. 1963 *Laminar Boundary Layers*. Oxford University Press.

Sivashinsky, G. I. 1977 Diffusional-thermal theory of cellular flames. *Combust. Sci. Technol.* **15**, 137–145.

Weatherburn, C. E. 1947 *Differential Geometry of Three Dimensions*. Cambridge University Press.

Williams, F. A. 1985 *Combustion Theory*. Benjamin/Cummings.

Yao, J. & Stewart, D. S. 1996 On the dynamics of multi-dimensional detonation. *J. Fluid Mech.* **309**, 225–275.